



**HAL**  
open science

## **Structural and Functional Analyses Explain Pea KAI2 Receptor Diversity and Reveal Stereoselective Catalysis During Signal Perception**

Angelica M Guercio, Salar Torabi, David Cornu, Marion Dalmais, Abdelhafid Bendahmane, Christine Le Signor, Jean-Paul Pillot, Philippe Le Bris, François-Didier Boyer, Catherine Rameau, et al.

► **To cite this version:**

Angelica M Guercio, Salar Torabi, David Cornu, Marion Dalmais, Abdelhafid Bendahmane, et al.. Structural and Functional Analyses Explain Pea KAI2 Receptor Diversity and Reveal Stereoselective Catalysis During Signal Perception. 2021. hal-03366101

**HAL Id: hal-03366101**

**<https://hal.science/hal-03366101v1>**

Preprint submitted on 7 Oct 2021

**HAL** is a multi-disciplinary open access archive for the deposit and dissemination of scientific research documents, whether they are published or not. The documents may come from teaching and research institutions in France or abroad, or from public or private research centers.

L'archive ouverte pluridisciplinaire **HAL**, est destinée au dépôt et à la diffusion de documents scientifiques de niveau recherche, publiés ou non, émanant des établissements d'enseignement et de recherche français ou étrangers, des laboratoires publics ou privés.

1       **Structural and Functional Analyses Explain Pea KAI2 Receptor Diversity and Reveal**  
2                               **Stereoselective Catalysis During Signal Perception**

3  
4   Angelica M. Guercio<sup>1</sup>, Salar Torabi<sup>2</sup>, David Cornu<sup>3</sup>, Marion Dalmais<sup>4</sup>, Abdelhafid Bendahmane<sup>4</sup>,  
5   Christine Le Signor<sup>5</sup>, Jean-Paul Pillot<sup>6</sup>, Philippe Le Bris<sup>6</sup>, François-Didier Boyer<sup>7</sup>, Catherine  
6   Rameau<sup>6</sup>, Caroline Gutjahr<sup>2</sup>, Alexandre de Saint Germain<sup>6\*</sup>, and Nitzan Shabek<sup>1\*</sup>

7  
8   <sup>1</sup> Department of Plant Biology, University of California – Davis, Davis, CA 95616

9  
10   <sup>2</sup> Plant Genetics, TUM School of Life Sciences, Technical University of Munich (TUM), 85354  
11   Freising

12  
13   <sup>3</sup> Université Paris-Saclay, CEA, CNRS, Institute for Integrative Biology of the Cell (I2BC), 91198,  
14   Gif-sur-Yvette, France.

15  
16   <sup>4</sup>Institute of Plant Sciences Paris-Saclay (IPS2), INRAE, CNRS, Université Paris-Sud, Université  
17   d'Evry, Université Paris-Diderot, 91405 Orsay, France

18  
19   <sup>5</sup>Agroécologie, AgroSup Dijon, INRAE, Univ Bourgogne, Univ Bourgogne Franche-Comté,  
20   21000 Dijon, France.

21  
22   <sup>6</sup> Institut Jean-Pierre Bourgin, INRAE, AgroParisTech, Université Paris-Saclay, 78000, Versailles,  
23   France

24  
25   <sup>7</sup> Université Paris-Saclay, CNRS, Institut de Chimie des Substances Naturelles, UPR 2301, 91198,  
26   Gif-sur-Yvette, France

27  
28   \*Correspondence should be addressed to: [nshabek@ucdavis.edu](mailto:nshabek@ucdavis.edu) , [Alexandre.De-Saint-](mailto:Alexandre.De-Saint-Germain@inrae.fr)  
29   [Germain@inrae.fr](mailto:Germain@inrae.fr)

31 **Abstract:**

32 KAI2 are plant  $\alpha/\beta$  hydrolase receptors, which perceive smoke-derived butenolide signals  
33 (karrikins) and putative endogenous, yet unidentified phytohormones (KAI2-ligands, KLs). The  
34 number of functional KAI2 receptors varies among plant species. It has been suggested that *KAI2*  
35 gene duplication and sub-functionalization plays an adaptative role for diverse environments or  
36 ligand diversification by altering the receptor responsiveness to specific KLs. Legumes represent  
37 one of the largest families of flowering plants and contain many essential agronomic crops. Prior  
38 to legume diversification, *KAI2* underwent duplication, resulting in *KAI2A* and *KAI2B*. Integrating  
39 plant genetics, ligand perception and enzymatic assays, and protein crystallography, we  
40 demonstrate that *Pisum sativum* KAI2A and KAI2B act as receptors and enzymes with divergent  
41 ligand stereoselectivity. KAI2B has a stronger affinity than KAI2A towards the KAI2-ligand (-)-  
42 GR24 and remarkably hydrolyses a broader range of substrates including the strigolactone-like  
43 isomer (+)-GR24. We determine the crystal structures of PsKAI2B in apo and butenolide-bound  
44 states. The biochemical and structural analyses as well as recorded mass spectra of KAI2s reveal  
45 a transient intermediate on the catalytic serine and a stable adduct on the catalytic histidine, further  
46 illuminating the role of KAI2 not only as receptors but also as *bona fide* enzymes. Our work  
47 uncovers the stereoselectivity of ligand perception and catalysis by evolutionarily diverged KAI2  
48 receptors in KAR/KL signaling pathways and proposes adaptive sensitivity to KAR/KL and  
49 strigolactone phytohormones by KAI2B.

50  
51  
52  
53  
54  
55  
56

57 **Introduction**

58  
59 Karrikins (KARs) are a family of butenolide small molecules produced from the combustion of  
60 vegetation and are bio-active components of smoke (1–3). These molecules are capable of  
61 inducing germination of numerous plant species, even those not associated with fire or fire-prone  
62 environments such as *Arabidopsis* (1–6). Through studies in *Arabidopsis*, KAR sensitivity was  
63 shown to be dependent on three key proteins: a KAR receptor  $\alpha/\beta$  hydrolase KARRIKIN  
64 INSENSITIVE2 (KAI2), an F-box MORE AXILLARY GROWTH 2 (MAX2) component of the  
65 Skp1-Cullin-F-box (SCF) E3 ubiquitin ligase, and the target of ubiquitination and degradation, the  
66 transcriptional corepressor SMAX1/SMXL2 (7–11). An increasing number of studies shows that  
67 the KAR signaling components are involved in the regulation of a number of plant developmental  
68 processes including seedling development, leaf shape, cuticle formation, and root development (8,  
69 12–15). Furthermore, they play critical roles in arbuscular mycorrhiza symbiosis and abiotic stress  
70 response (16–18).

71 The striking similarities between KAR and strigolactone (SL) signaling pathways have been  
72 the focus of an increasing number of studies. Both SLs and KARs share a similar butenolide ring  
73 structure but instead of the KAR pyran moiety, the butenolide is connected via an enol ether bridge  
74 to either a tricyclic lactone (ABC rings) in canonical SLs, or to a structural variety in non-canonical  
75 SLs (19, 20). The receptor for SL, DWARF14 (D14) shares a similar  $\alpha/\beta$  hydrolase fold as KAI2  
76 and a parallel signaling cascade requiring the function of the MAX2 ubiquitin ligase and  
77 degradation of corepressors (SMXL6, 7 and 8), which belong to the same protein family as  
78 SMAX1/SMXL2 (7, 8, 11, 21). Unlike KARs, SLs are plant hormones that act endogenously, but  
79 were also found to be exuded by plant roots. SLs affect diverse responses such as hyphal branching  
80 of arbuscular mycorrhizal (AM) fungi to enhance the efficiency of root colonization, germination

81 of root parasitic plant species, shoot branching, lateral root formation, primary root growth,  
82 secondary growth in the stem, leaf senescence, and adventitious root formation (22–28). Notably,  
83 KAI2 family receptors have undergone numerous duplication events within various land plant  
84 lineages. D14 was found to be an ancient duplication in the KAI2 receptor in the seed plant lineage  
85 followed by sub-functionalization of the receptor, enabling SL perception (29–32). This sub-  
86 functionalization has been highlighted by the observations that D14 and KAI2 are not able to  
87 complement each other's functions in planta (33–37). While the role of the D14 receptor in SL  
88 signaling is better established, KAI2 receptors and KAR signaling are less understood. A central  
89 question in receptor diversity has been the evolutionary purpose and functional significance of  
90 *KAI2* duplication events, including but not limited to the event that led to the distinct SL receptors  
91 D14s. D14s and KAI2s contain over a 70% sequence similarity but confer unique functions in  
92 plant. Notably, within the KAI2 family the substitution of a few amino acids within the ligand  
93 binding site can alter ligand specificity between KAI2 duplicated copies in *Brassica tournefortii*  
94 and *Lotus japonicus* (35, 38). Additionally, given that KAR signaling governs diverse  
95 developmental processes including those unrelated to fire, KAI2s are thought to perceive  
96 endogenous ligands, which remain elusive and tentatively named KAI2-Ligands (KLs) (29, 30,  
97 37, 39). Therefore, the ability to alter the specificity of KAI2 receptors to different ligands is likely  
98 to be correlated to their ability to perceive distinct KLs. Thus far, several crystal structures of  
99 KAI2/D14 receptors have been reported and led to a greater understanding of receptor-ligand  
100 perception towards certain ligands (9, 21, 32, 34, 40–42). However, the divergence between  
101 duplications of KAI2 receptors to confer altered ligand perception and hydrolysis specificities has  
102 been only partially addressed for few plant species at the physiological and biochemical level, and  
103 a detailed structural examination is still missing (34–36, 38).

104 Legumes represent one of the largest families of flowering plants and contain many essential  
105 crops. Beyond their agronomic value, most legume species are unique among plants because of  
106 their ability to fix nitrogen by utilizing symbiosis with rhizobia, in addition to AM fungi symbiosis.  
107 Because of the potential functional diversification and specialization of KAI2-ligands, in this  
108 study, we examined the physiological and biochemical functions of divergent KAI2 receptors in a  
109 legume, using *Pisum sativum* (*Ps*) as a model. We found that *Pisum sativum* expresses three  
110 distinct *KAI2* homologues, two of which, *KAI2A* and *KAI2B* have sub-functionalized, while *KAI2C*  
111 is a pseudogene. Using comprehensive biochemical characterization, we show that these divergent  
112 receptors display distinct ligand sensitivities and hydrolytic activities. We further substantiate  
113 these findings *in planta* by investigating the sensitivities to ligands on hypocotyl elongation in  
114 *Arabidopsis* transgenic complementation lines expressing PsKAI2A and PsKAI2B, as well as  
115 studying phenotypic effects in *Pisum sativum* wild-type and *kai2* mutants. Strikingly, KAI2B, was  
116 more reactive than KAI2A towards SL/KARs stereoisomers. The diverged receptor was able to  
117 cleave strigolactone synthetic analog (+)-GR24, although not to the same extent as D14/RMS3,  
118 suggesting that PsKAI2B evolved the ability to sense SL-like ligands. To further address this  
119 notion, we determine the structure of an evolutionarily diverged PsKAI2B in *apo* and a unique  
120 butenolide-bound state at high resolution (1.6 Å and 2.0 Å, respectively). Unlike the D14  $\alpha/\beta$   
121 hydrolase, mass spectrometry analysis and structural examination reveal a mode of ligand  
122 perception and hydrolysis by PsKAI2, that involves an intermediate step in which the catalytic  
123 serine is transiently bound to a moiety of the ligand and then form a stable adduct with the catalytic  
124 histidine. Altogether, in this study we identify and characterize divergent KAI2 receptors, reveal  
125 their distinct function and ligand sensitivities and illuminate KAI2s enzymatic mechanism. Better  
126 understanding of the evolution of plant  $\alpha/\beta$  hydrolase receptors and their functional adaptation in

127 KAR/KL/SL sensing, in particular in a key crop, will have far-reaching impact on the implications  
128 of KAR/KL signaling pathways in agro-systems and food security.

129

## 130 **Results**

131

### 132 ***Identification and characterization of the *Pisum sativum* KAI2 genes***

133 To characterize the karrikin sensing machinery in legumes, we built a phylogenetic tree of  
134 representative legume *KAI2*s. *KAI2* has undergone two independent duplication events in the  
135 legume lineage prior to its diversification followed by the loss of *KAI2C* in the hologalegina clade  
136 resulting in distinct *KAI2A* and *KAI2B* protein receptors (**Fig. 1a** and **Fig. S1**) (38). We focused  
137 on the hologalegina representative *Pisum sativum* for which a high-quality, annotated genome  
138 sequence has been recently obtained (43). We identified three *KAI2* homologs in the pea genome  
139 (43) that clearly group within the core *KAI2* clade by phylogenetic analysis. One (Psat4g083040)  
140 renamed *PsKAI2B*, grouped in the same subclade as the legume *KAI2Bs* (including *Lotus*  
141 *japonicus*, *Lj*, *KAI2B* (38)), and two Psat2g169960 and Psat3g014200 respectively termed  
142 *PsKAI2A* and *PsKAI2C*, in the same subclade as the legume *KAI2As* (including *LjKAI2A* (38))  
143 (**Fig. 1a** and **Fig. S1**). *PsKAI2C* was detected by PCR in the genomic, but not the cDNA, and  
144 appear to be pseudogene because the predicted encoded protein is truncated at 128 amino acids  
145 (aa) due to a premature stop codon at 387 nucleotides after the translation initiation site (**Fig. 1b**).  
146 By cloning the *PsKAI2A* coding sequence (CDS) we identified two transcripts for this gene,  
147 corresponding to two splice variants (**Fig. 1b** and **Fig. S2**). The transcript *PsKAI2A.1* results from  
148 intron splicing and encodes a protein of 305 aa. Thus, this protein shows a C-terminal extension  
149 of 33 aa similar to *LjKAI2A* (**Fig. S2**), missing in other *KAI2* proteins. The *PsKAI2A.2* transcript  
150 arises from the intron retention and shows a premature STOP codon two nucleotides after the end

151 of the first exon. This leads to a 272 aa protein representing a similar size to other KAI2s described  
152 (**Fig. 1b** and **Fig. S2**). Due to the similar size, lack of introns, and evolutionary conservation of the  
153 residues contained in the PsKAI2A.2 protein, PsKAI2A hereafter will refer to the PsKAI2A.2  
154 protein. From this analysis, it is clear that the KAI2 clade has undergone an independent  
155 duplication event in the legume lineage, resulting in two functional KAI2A and KAI2B forms (**Fig.**  
156 **S1a-b**). To examine potential functional divergence between the PsKAI2A.2 and PsKAI2B forms,  
157 we first analyzed the aa sequences and identified notable alterations in key residues, of which  
158 numerous are likely to be functional changes as indicated in later analyses (**Fig. S3**). To further  
159 characterize divergence of these genes, we studied their expression patterns in various tissues of  
160 the *Pisum* plant (**Fig. 1c-d**). Interestingly, *PsKAI2A* was ten-fold more highly expressed in  
161 comparison to *PsKAI2B* and the expression in the roots differed between the two forms, suggesting  
162 sub-functionalization between transcriptional regulatory sequences of *PsKAI2A* and *PsKAI2B*.

163

#### 164 ***Identification and phenotypic examination of Pskai2a and Pskai2b TILLING mutants***

165 To investigate the function of *PsKAI2A* and *PsKAI2B*, mutants in both genes were identified via  
166 Targeting-Induced Local Lesions IN Genomes (TILLING) using the mutagenized Caméor  
167 population (44, 45). Twenty mutations in *PsKAI2A* and sixteen mutations in *PsKAI2B* were  
168 identified (**Table S1**). Among them, five of the *PsKAI2A* and three of the *PsKAI2B* mutations were  
169 predicted as non-synonymous and may result in mutated amino acids that compromise the protein  
170 function (**Table S1, Fig. 2a, Fig. S4**). The comparison between wild-type and *Pskai2* single  
171 mutants revealed no detectable shoot architecture differences in either branch number or in plant  
172 height. The double mutant *Pskai2a-6 Pskai2b-3* showed a reduced height and decreased branching  
173 (**Fig. S5a-c**). Similar to the other legume *L. japonicus* and in contrast to *Arabidopsis thaliana* (38,



174 46), the root hair length of the double mutant *Ps kai2a-6 Ps kai2b-3* in pea is not significantly  
175 different from wild-type. Together, under our growth conditions, KAI2 requirement for root hair  
176 elongation differs among plant species/families and may be absent from legumes. (**Fig. S5d, e**).

177

178 ***Karrikin signaling reporter DLK2 expression is mediated by KAI2s in P. sativum roots in a***  
179 ***ligand-specific manner***

180 It was recently shown, in *L. japonicus* that the root system architecture can be modulated by KAR<sub>1</sub>  
181 but not by KAR<sub>2</sub> treatment, and the expression of the KAR signaling marker gene, *DLK2* in roots,  
182 was responsive only to KAR<sub>1</sub> but not to KAR<sub>2</sub> (38). Furthermore, LjKAI2A and LjKAI2B have  
183 distinct ligand-binding specificities since LjKAI2A but not LjKAI2B can perceive (–)-GR24 *in*  
184 *vitro*. This alteration in perception depends on the divergent amino acid F157/W158 within the  
185 ligand binding pocket, and indeed in roots, LjKAI2A but not LjKAI2B can induce *DLK2*  
186 expression in response to (–)-GR24 (38). Intriguingly, because F157/W158 amino acid difference  
187 between KAI2A and KAI2B is not conserved across most legumes, this raises the question how  
188 pea roots respond to the range of artificial ligands. Thus, we treated pea wild-type, *kai2a-6*, *kai2b-*  
189 *3*, and *kai2a-6 kai2b-3* double mutant roots with KAR<sub>1</sub>, KAR<sub>2</sub>, (+)-GR24, and (–)-GR24 and  
190 performed RT-qPCR analysis of *PsDLK2* transcript accumulation (**Fig. 2b**). Similar to *L.*  
191 *japonicus*, *DLK2* was induced in pea wild-type roots only in response to KAR<sub>1</sub> but not to KAR<sub>2</sub>.  
192 Interestingly, without treatment, *PsDLK2* expression was significantly reduced in both single  
193 mutants (*kai2a-6* and *kai2b-3*) indicating that *KAI2A* and *KAI2B* are not fully redundant and even  
194 more so in the double mutant (*kai2a-6 kai2b-3*) (**Fig. 2b**). This expression pattern strongly suggests  
195 that PsKAI2A and PsKAI2B functionally mediate KAR signaling and validates that the *kai2a-6*  
196 and *kai2b-3* mutants perturb protein function. Surprisingly, in response to KAR<sub>1</sub>, *Ps kai2a-6* shows

197 only a minor induction of *PsDLK2*, whereas *Ps kai2b-3* shows no *PsDLK2* induction. Given that  
198 both *PsKAI2A* and *PsKAI2B* transcripts accumulated to similar levels (**Fig. 2c, d**), these data  
199 suggest that either PsKAI2B protein accumulate to higher levels than PsKAI2A or it is more active  
200 in KAR<sub>1</sub> perception. In all genotypes, *PsDLK2* was induced by (-)-GR24 treatment, which is  
201 consistent with previous studies in Arabidopsis where (-)-GR24 also acts as ligand for the SL  
202 receptor D14 (46, 47). Unlike the observations with *L. japonicus* (38), all pea genotypes showed a  
203 significant induction of *DLK2* expression in response to (-)-GR24, with a significantly stronger  
204 induction in the wild-type and the single mutants as compared to the double mutant. Thus, in pea,  
205 (-)-GR24 is not only perceived by KAI2 but to some extent also by the SL receptor D14, similar  
206 to previous observations in Arabidopsis (46). However, we cannot exclude the possibility that the  
207 mutated proteins are still able to perceive (-)-GR24, even though they lost sensitivity to KAR<sub>1</sub>.

208

### 209 *PsKAI2A, but not PsKAI2B, rescues inhibition of hypocotyl elongation in Arabidopsis kai2* 210 *mutants*

211 Since we could not distinguish a possible differential sensitivity of PsKAI2A and PsKAI2B in the  
212 pea background (as previously observed in *L. japonicus* (38)), we performed a cross-species  
213 complementation by transforming the Arabidopsis *htl-3* (also known as *kai2*) mutant with  
214 *PsKAI2A.2* and *PsKAI2B* (**Fig. 3**). The genes were expressed as fusions with *mCitrine* or *GUS* and  
215 driven by the native *AtKAI2* promoter (*pAtKAI2*) (**Fig. S6b-c**). To test protein functionality we  
216 performed the widely used hypocotyl elongation assay (33, 39) under low light conditions, which  
217 causes an elongated hypocotyl phenotype of the *htl-3* mutant when compared to the wild-type  
218 Columbia (Col-0). Remarkably, all transgenes, except *PsKAI2B*, completely or partially restored  
219 hypocotyl length of *htl-3* to the wild-type length (**Fig. 3**). Also interestingly, all lines (even *htl-3*),

220 except those complemented with PsKAI2A responded to (-)-GR24 (**Fig. 3**). We repeated the  
221 complementation for the *kai2-2* mutant in the Landsberg erecta (Ler) background. The data  
222 confirmed that the two *PsKAI2A* splice forms restored the reduced hypocotyl length in *kai2-2* but  
223 the proteins did not mediate responses to (-)-GR24, whereas PsKAI2B did not restore the wild-  
224 type hypocotyl length but mediated a response to (-)-GR24 (**Fig. S6**). Interestingly, these results  
225 suggest that PsKAI2A can perceive endogenous KL in Arabidopsis but does not perceive the  
226 synthetic (-)-GR24. In contrast, PsKAI2B is unable to perceive KL but is sensitive to (-)-GR24.  
227 These results propose that *PsKAI2A* is the functional orthologue of Arabidopsis *KAI2* while  
228 PsKAI2B has diverged and adapted to perceive different ligands.

229

### 230 *Altered ligand binding specificity and activity between PsKAI2s*

231 To further investigate the distinct ligand selectivity, we purified PsKAI2 recombinant proteins and  
232 studied their ligand-interaction and ligand-enzymatic activities using various complementary  
233 assays (**Fig. 4-5** and **Fig. S7-S9**). We first examined PsKAI2A.2 and PsKAI2B ligand interactions  
234 via the thermal shift assay (Differential Scanning Fluorimetry, DSF) with various KAI2/D14  
235 family ligands including (+) and (-)-GR24 enantiomers (also known as GR24<sup>5DS</sup> and GR24<sup>ent-5DS</sup>,  
236 respectively), and (+)- and (-)-2'-*epi*-GR24 (also known as GR24<sup>ent-5DO</sup> and GR24<sup>5DO</sup>,  
237 respectively) (47) (**Fig. 4c-f**, **Fig. S8**). DSF analyses revealed an increased shift in stability in the  
238 presence of (-)-GR24 for PsKAI2B as compared to PsKAI2A which has little to no alteration (**Fig.**  
239 **4c-f**). The other ligands and enantiomers induce no detectable shift in stability for either receptor.  
240 An extensive interaction screen using intrinsic fluorescence confirmed that only the (-)-GR24  
241 stereoisomer interacts with PsKAI2 proteins (**Fig. 4b** and **Fig. S9**), and further corroborating the  
242 results of the Arabidopsis hypocotyl elongation and the DSF assays. The calculated  $K_d$  shows a

243 higher affinity for (-)-GR24 for PsKAI2B ( $K_d = 89.43 \pm 12.13 \mu\text{M}$ ) than PsKAI2A ( $K_d = 115.40 \pm$   
244  $9.87 \mu\text{M}$ ).

245 Because the structural similarity between KAI2s and D14s  $\alpha/\beta$  hydrolases in particular the  
246 conserved serine catalytic triad signature of these receptors, we examine the potential catalytic  
247 function of KAI2s. The hydrolytic activity of the PsKAI2 proteins towards distinct ligands was  
248 quantified in comparison to AtD14, AtKAI2, and RMS3. The proteins were incubated with (+)-  
249 GR24, (-)-GR24, (+)-2'-*epi*-GR24 and (-)-2'-*epi*-GR24 in presence of 1-indanol as an internal  
250 standard, followed by ultraperformance liquid chromatography (UHPLC)/UV DAD analysis (**Fig.**  
251 **5**). Interestingly, PsKAI2A can only cleave (-)-GR24, while PsKAI2B is able to cleave (+)-GR24,  
252 (-)-GR24 and (-)-2'-*epi*-GR24 stereoisomers. Among the tested ligands, all enzymes show  
253 reduced activity towards (+)-2'-*epi*-GR24, and among the KAI2s, PsKAI2A had no detectable  
254 activity for (+)-2'-*epi*-GR24. These results strongly indicate that PsKAI2s have distinct  
255 stereoselectivity, and PsKAI2B appears to be more reactive. To further investigate the hydrolysis  
256 kinetics of PsKAI2 proteins, we performed an enzymatic assay with pro-fluorescent probes that  
257 were previously designed for detecting SL hydrolysis (36, 48) (**Fig. 4g-h**). As expected, PsKAI2A  
258 shows no activity towards the probe ( $\pm$ )-GC240, similar to AtKAI2, as previously reported (48).  
259 Strikingly, PsKAI2B is able to cleave ( $\pm$ )-GC240, suggesting yet again that unlike PsKAI2A,  
260 PsKAI2B has a ligand stereoselectivity that is similar to AtD14 and RMS3 (**Fig. 4g**). Since probes  
261 without a methyl group, such as dYLG, can serve as the hydrolysis substrates for AtKAI2 (49),  
262 we tested the activity of KAI2s and D14s using the ( $\pm$ )-GC486 probe bearing no methyl on D-ring.  
263 Notably, PsKAI2B, RMS3, and AtD14 were able to effectively hydrolyze ( $\pm$ )-GC486, whereas  
264 PsKAI2A and AtKAI2 showed little activity (**Fig. 4h**). Nonetheless, PsKAI2A and AtKAI2 also  
265 exhibit a biphasic time course of fluorescence, consisting of an initial phase, followed by a plateau

266 phase. Comparative analysis of the kinetic profiles shows that PsKAI2B, RMS3 and AtD14 display  
267 a higher plateau (1  $\mu\text{M}$  versus 0.3  $\mu\text{M}$  of DiFMU, **Fig. 4h**). Taken together the comparative kinetic  
268 analysis substantiates the distinct function of PsKAI2B compared to PsKAI2A not only highlights  
269 the unique similarity of PsKAI2B to SL receptors (8, 10, 36, 40–42, 48, 50) rather than karrikin  
270 receptors (8–10, 13, 34–36, 38, 49), but may also offer new insights into the missing link between  
271 Karrikin and SL by diverged KAI2s.

272

### 273 *Structural insights into divergence of legume KAI2A and KAI2B*

274 To elucidate the structural basis for the differential ligand selectivity between KAI2A and KAI2B,  
275 we determined the crystal structure of PsKAI2B at 1.6 Å resolution (**Fig. 6** and **Table S2**). The  
276 PsKAI2B structure shares the canonical  $\alpha/\beta$  hydrolase fold and comprises base and lid domains  
277 (**Fig. 6a**). The core domain contains seven-stranded mixed  $\beta$ -sheets ( $\beta 1$ – $\beta 7$ ), five  $\alpha$ -helices ( $\alpha A$ ,  
278  $\alpha B$ ,  $\alpha C$ ,  $\alpha E$  and  $\alpha F$ ) and five  $3_{10}$  helices ( $\eta 1$ ,  $\eta 2$ ,  $\eta 3$ ,  $\eta 4$ , and  $\eta 5$ ). The helical lid domain (residues  
279 124–195, **Fig. S3**) is positioned between strands  $\beta 6$  and  $\beta 7$  and forms two parallel layers of V-  
280 shaped helices ( $\alpha D 1$ –4) that create a deep pocket area adjoining the conserved catalytic Ser-His-  
281 Asp triad site (**Fig. 6b** and **Fig. S3**). Despite the sequence variation (77% similarity between  
282 PsKAI2B and AtKAI2, **Fig. S3**), we did not observe major structural rearrangements between  
283 PsKAI2B and the previously determined Arabidopsis KAI2 structure (51) as shown by an Root  
284 Mean Squared Deviation (RMSD) of 0.35 Å for superposition of backbone atoms (**Fig. 6b**).  
285 Nonetheless, further structural comparative analyses have identified two residue alterations in  
286 positions 129 and 147 within the lid domain which appear to slightly alter the backbone atoms and  
287 generally distinguish legume KAI2 proteins from KAI2s in other species (**Fig. S3** and **Fig. 6b**).  
288 The asparagine residue in position 129 is more unique to legume KAI2As, and the legume alanine

289 or serine in position 147 has diverged from bulky polar residues compared to other KAI2s.  
290 Therefore, it is likely that these amino acids variations play role in downstream events rather than  
291 directly modulate distinct ligand perception.

292 To further determine the differential ligand specificity between PsKAI2A and PsKAI2B, we  
293 utilized the PsKAI2B crystal structure reported here to generate a high probability 3D model for  
294 PsKAI2A. As expected, PsKAI2A structure exhibits a similar backbone atom arrangement (RMSD  
295 of 0.34 Å) that parallels the PsKAI2B structure (**Fig. 7a**). Nonetheless, we identified eight  
296 significant divergent amino acids between the two structures including residues involved in  
297 forming the ligand binding pocket as well as solvent-exposed regions (**Fig. 7b-d** and **Fig. S10a-**  
298 **b**). Because these variants are evolutionarily conserved across legumes, the analysis of the  
299 underlined residues not only distinguishes between KAI2A and KAI2B in *Pisum* but can be  
300 extrapolated to other legume KAI2A/B diverged proteins. Structural comparative analysis within  
301 the ligand-binding pocket shows divergent solvent accessibility between PsKAI2A and PsKAI2B  
302 (**Fig. 7b**). PsKAI2B exhibits a structural arrangement that results in a larger volume of the  
303 hydrophobic pocket (125.4 Å<sup>3</sup>) yet with a smaller entrance circumference (30.3 Å) than PsKAI2A  
304 (114.8 Å<sup>3</sup> and 33.6 Å, respectively, **Fig. 7b**). Further *in silico* docking experiments of (-)-GR24  
305 with PsKAI2B results in a successful docking of the ligand that is totally buried in the pocket and  
306 positioned in a pre-hydrolysis orientation nearby the catalytic triad. In contrast, docking  
307 experiments of (-)-GR24 with PsKAI2A results in more restricted interaction where the ligand is  
308 partially outside the pocket (**Fig. S10c**). Notably, there are five key residues that are found to  
309 directly alter the pocket morphology (**Fig. 7c** and **Fig. S10a-b**). Among these residues,  
310 L160/S190/M218 in PsKAI2A and the corresponding residues, M160/L190/L218 in PsKAI2B are  
311 of particular interest because of their functional implications in the pocket volume and solvent

312 accessibility (**Fig. 7d**). Interestingly, the variant in position 218 places it in the center of the Asp  
313 loop (D-loop, region between  $\beta$  7 and  $\alpha$ E, **Fig. 7c-d**), that has been recently suggested to impact  
314 D14 protein-protein interactions in SL signaling (52, 53). Residues 160 and 190 are of great  
315 interest because of their direct effect on ligand accessibility and binding pocket size. Residue 160  
316 is positioned at the entrance of the ligand-binding pocket in helix  $\alpha$ D2, thus the substitution of  
317 leucine (L160 in KAI2A) to methionine (M160 in KAI2B) results in modifying the circumference  
318 of PsKAI2B pocket entrance (**Fig. 7b-d**). While both L160 and M160 represent aliphatic non-polar  
319 residues, the relative low hydrophobicity of methionine as well as its higher plasticity are likely to  
320 play a major role in modifying the ligand pocket. The conserved divergence in residue 190 (S190  
321 in PsKAI2A and L190 in PsKAI2B, **Fig. 7d**) is positioned in helix  $\alpha$ D4 and represents a major  
322 structural arrangement at the back of the ligand envelope. Because leucine has moderate flexibility  
323 compared to serine and much higher local hydrophobicity, this variation largely attributes to the  
324 changes in the pocket volume as well as fine-tunes available ligand orientations.

325 To further examine whether the diverged residues directly impact ligand perception. We produced  
326 the recombinant reciprocal swap mutants PsKAI2A.2<sup>L160M, S190L</sup> and PsKAI2B<sup>M160L, L190S</sup>, and  
327 tested their sensitivity to selected ligands by DSF. Remarkably, the swap of PsKAI2A.2 and  
328 PsKAI2B at residues 160 and 190 resulted in a loss of sensitivity of PsKAI2B<sup>M160L, L190S</sup> towards  
329 (-)-GR24 ligand, yet with no gain of sensitivity of PsKAI2A.2<sup>L160M, S190L</sup> (**Fig. S11**). This  
330 demonstrates that the variation in residues 160 and 190 in KAI2s are necessary for ligand  
331 perception and selectivity but may not be entirely sufficient for PsKAI2B perception of (-)-GR24.  
332 Notably, structural analysis of the ligand-envelopes of PsKAI2A.2<sup>L160M, S190L</sup> and PsKAI2B<sup>M160L,</sup>  
333 <sup>L190S</sup> in comparison to their WT counterparts further corroborates the adapted pocket size in  
334 PsKAI2B<sup>M160L, L190S</sup>, which explain the observed loss of sensitivity to (-)-GR24 (**Fig. S11e**).

335

336 ***Structural and functional elucidation of ligand hydrolysis mechanism by PsKAI2B receptor***

337 To examine the molecular interaction of PsKAI2B with the enantiomer (–)-GR24, we co-  
338 crystallized and determined the structure of PsKAI2B-(–)-GR24 at 2.0 Å resolution (**Fig. 8a** and  
339 **Table S2**). Electron density map analysis of the ligand-binding pocket revealed the existence of a  
340 unique ring-shaped occupancy that is contiguously linked to the catalytic serine (S95) (**Fig. 8a-b**).  
341 The structural comparison of the backbone atoms between apo-PsKAI2B and PsKAI2B-(–)-GR24  
342 did not reveal significant differences (**Fig. S12a**) and is in agreement with previously reported *apo*  
343 and ligand bound D14/KAI2 crystal structures (9, 10, 21, 32, 41). This similarity suggests that a  
344 major conformational change may indeed occur as proposed for D14 (53). It may happen after the  
345 nucleophilic attack of the catalytic serine and the (–)-GR24 cleavage which is likely to be a highly  
346 unstable state for crystal lattice formation. Further analysis suggests that the 5-hydroxy-3-  
347 methylbutenolide (D-OH ring), resulting from the (–)-GR24 cleavage, is trapped in the catalytic  
348 site (**Fig. S12b-d**). The lack of a defined electron density fitting with the tricyclic lactone (ABC  
349 ring) may exclude the presence of the intact GR24 molecule. Other compounds present in the  
350 crystallization condition were tested for their ability to occupy the S95-contiguous density, and the  
351 D-OH group of (–)-GR24 demonstrated the highest calculated correlation coefficient (CC) score  
352 and the best fit in the PsKAI2B co-crystal structure (**Fig. S12c**). Additional tests of D-OH binding  
353 including *in silico* docking simulations and analyses revealed a high affinity for D-OH in a specific  
354 orientation and in agreement with the structure presented here (**Fig. S12d**). The most probable  
355 orientation of the D-OH positions the methyl group (C4') together with the hydroxyl group of D-  
356 OH towards the very bottom/back of the pocket near the catalytic serine, where the O5'' atom is  
357 coordinated by both N atoms of F26 and V96 (**Fig. 8b-c**). The hemiacetal group (C2') of D-OH is



358 oriented towards the access groove of the pocket with angles (between carbon and oxygen atoms)  
359 supporting the captured D-OH in an orientation in which cleavage of the intact (–)-GR24 may have  
360 taken place. The C5' of D-OH appears to form a covalent bond with O $\gamma$  of S95 (dark gray line in  
361 **Fig. 8c**) and generates a tetrahedral carbon atom. The overall positioning of this molecule is strictly  
362 coordinated by F26, H246, G25, and I193 residues. Notably, the electron density around the S95  
363 does not display an open D-OH group (2,4,4,-trihydroxy-3-methyl-3-butenal as previously  
364 described for OsD14 (21)) that could directly result from the nucleophilic attack event, but rather  
365 more closely corresponds to a cyclized D-OH ring linked to the S95. The D-OH ring is likely to  
366 be formed by water addition to the carbonyl group at C2' that is generated after cleavage of the  
367 enol function and cyclization to re-form the butenolide (**Fig. 8d**). Based on the suggested  
368 mechanism of SL hydrolysis by D14 (36, 48, 50, 53), we propose that the formation of the S95-  
369 adduct serves as a highly transient intermediate before its transfer to the catalytic histidine residue.  
370 Therefore, to further examine (–)-GR24 catalysis by PsKAI2s, we recorded mass spectrometry  
371 (MS) spectra under denaturing conditions with PsKAI2B and PsKAI2A. As expected, a mass shift  
372 occurred corresponding to an intermediate covalently bound to PsKAI2s (**Fig S13a-d**). Following  
373 digestion, a peptide with additional mass of 96 Da was detected on the catalytic residue H246,  
374 further corroborating the transient nature of S95-adduct that was capture in the crystal structure  
375 (**Fig. S13e-f**). Collectively, the crystal structure of PsKAI2B bound to GR24 and the MS data show  
376 transient and stable intermediates attached to S95 and H246 of the catalytic triad and reveal the  
377 mode of action of KAI2 as receptors and enzymes (**Fig. 8d**).

## 378 **Discussion**

379 The coevolution between receptors and ligands in diverse environments throughout plant evolution  
380 is of wide interest in many biological fields. In particular, characterization of the emerging  
381

382 karrikin/KL signaling in non-fire following plants has been of increasing importance in plant  
383 signaling at large. While there are many missing pieces in the karrikin/KL signaling puzzle, it is  
384 clear that KAI2 is the key sensor in this pathway(s). The striking evolutionary conservation of  
385 KAI2 receptors in all land plants is not fully explained by the limited natural occurrence of smoke-  
386 derived karrikin molecules as well as non-fire following species. Also, an increasing number of  
387 studies suggests that the functions of KAI2s are preserved to regulate plant development and  
388 response to stresses by perceiving KL signals from either internal or external sources. Most  
389 importantly, the intriguing potential dual function of KAI2s as receptors and enzymes remained  
390 largely elusive. Here, we identified and characterized the KAI2 receptors in pea (*P. sativum*) that  
391 serve as representatives to examine KAI2 sub-functionalization in legumes. The identification of  
392 both *PsKAI2A* and *PsKAI2B* genes corroborates the recent finding that the *KAI2* gene duplication  
393 event occurred in Papilionoidae before the diversification of legumes (38). The similarities in  
394 gene expression patterns are found between pea and *Lotus* with globally higher expression of  
395 *KAI2A* in comparison to *KAI2B* and higher expression *KAI2B* versus *KAI2A* in roots, depending  
396 on whether the plants are grown in pots or on Petri dishes. In the characterization of the PsKAI2  
397 TILLING mutant lines, the effects on branching and root hair phenotypes were not significant.  
398 Thus, future studies of pea *Ps kai2a/b* mutants will further delineate the distinct physiological  
399 functions, in particularly their symbiotic relationship with AM fungi and the differential expression  
400 patterns in the roots. Interestingly, both pea single mutants can induce the expression of *PsDLK2*  
401 in response to (-)-GR24, which is in agreement with the observation of (-)-GR24 perception by  
402 *L. japonicus* KAI2B (38) and substantiate the hindering effect of W158 in (-)-GR24 perception  
403 that is absent from pea PsKAI2s. Yet our DSF analyses suggest that PsKAI2B differs from its  
404 ortholog from *L. japonicus*, which is not destabilized by (-)-GR24 due to a rare phenylalanine to

405 tryptophan exchange at position 158 at the binding pocket (38). The arabidopsis complementation  
406 experiments with pea KAI2s verified the distinct functionalities of PsKAI2A and PsKAI2B,  
407 wherein PsKAI2A most closely resembles AtKAI2 complementation in hypocotyl elongation  
408 assays indicating sensitivity to the endogenous KL, while PsKAI2B and not PsKAI2A is able to  
409 rescue the sensitivity of the *htl-3* and *kai2-2* mutants to (-)-GR24.

410 The occurrences of molecular coevolution of ligands and their specialized receptors have been  
411 previously demonstrated for phytohormones such as SL (55), ABA (56), GA (57), and more  
412 recently, karrikins (35, 38). Even though the exact identity of KL remains to be revealed, it is  
413 thought that the ligands likely share a common chemical composition to SLs. As such, it has been  
414 recently shown that one enantiomer of the artificial SL analogue, *rac*-GR24, can function by  
415 binding KAI2 in Arabidopsis (9, 39, 49). Here we show that PsKAI2B can form stronger  
416 interactions with the enantiomer (-)-GR24, compared to PsKAI2A. Moreover, we found that while  
417 both KAI2s are active hydrolases, they have distinct binding affinity and stereoselectivity towards  
418 GR24 stereoisomers. These findings indicate that sub-functionalization of KAI2s via substitutions  
419 in only few amino acids can greatly alter ligand affinity, binding, enzymatic activity, and probably  
420 signaling with downstream partners (34, 38).

421 To better elucidate PsKAI2A/B molecular divergence and their dual receptor-enzyme function,  
422 we carried out extensive biochemical and structural studies. KAI2/D14 crystal structures have  
423 greatly impacted our understanding of their receptor ligand-binding pockets and their ability to not  
424 only accommodate, but also hydrolyze certain ligands (9, 21, 32, 34, 40–42). The crystal structure  
425 of legume PsKAI2B together with the PsKAI2A homology model reported here, further  
426 substantiates the structural basis of this differential ligand selectivity. We identified conserved key  
427 amino acid changes that alter the shape of the pocket and confer altered ligand specificities. These

428 atomic structures of legume KAI2 enabled us to analyze the distinction between key residues  
429 L160/S190/M218 in PsKAI2A and the corresponding residues M160/L190/L218 in PsKAI2B.  
430 Further swap experiments between residues 160 and 190 confirmed that these residues are  
431 necessary for the sensitivity of PsKAI2B for (-)-GR24, but not sufficient to bring PsKAI2A to  
432 similar sensitivities. These findings support recent *in planta* studies that demonstrate that residues  
433 160 and 190 are required for differential ligand specificity between *Lotus* KAI2A and KAI2B (38).  
434 Furthermore, the residue in position 190 was also identified in the parasitic plant *Striga*  
435 *hermonthica* as being involved in forming differential specificity pockets between the highly  
436 variable and functionally distinct HTLs (31, 32). While the changes in positions 160 and 190  
437 directly reshape the pocket morphology, the variant in position 218 is located in the center of the  
438 D-loop that has been suggested in downstream protein-protein interactions (52, 53). Therefore, the  
439 conserved substitution of KAI2A and KAI2B in M218 to L218 respectively across legumes may  
440 also contribute to downstream interaction(s). Based on the analogy with the D14-MAX2  
441 perception mechanism, the KAI2 receptor is likely to adopt different conformational states upon  
442 ligand binding and cleavage. As such, the identification of unique residue variations in the lid  
443 (between KAI2A and KAI2B, respectively in positions 129 and 147) reported here, infer a sub-  
444 functionalization in the receptor regions that are likely to be involved in MAX2 and/or SMAX1  
445 and/or SMXL2 downstream interactions. Therefore, it remains to be further elucidated whether  
446 these distinctive residues play a role in fine tuning the formation of the protein complex with  
447 MAX2-SMAX1/SMXL2.

448 The crystal structure of ligand-bound PsKAI2B provides a unique mechanistic view of  
449 perception and cleavage by KAI2s. Based on the crystallization conditions and following a detailed  
450 investigation of the electron density, we were able to overrule common chemicals and place the (-

451 )-GR24 D-OH ring with higher relative fitting values than other components. The absence of  
452 positive electron density peaks corresponding to the intact (-)-GR24, and thus the presence of only  
453 the D-OH ring, raise questions of whether the S95-D-OH adduct recapitulates a pre- or post-  
454 cleavage intermediate state of (-)-GR24. The possibility that the trapped molecule represents a  
455 post cleavage state is intriguing and may provide a new intermediate state where S95 is covalently  
456 linked to the cleavage product. As such, the S95-D-OH adduct suggested here could explain the  
457 single turnover cycle that was observed for KAI2s in this study. While early structural study of  
458 D14 hydrolysis also positioned the catalytic serine with a covalent adduct, (21) other studies of the  
459 single turnover activity of D14 suggest that a covalent intermediate is in fact formed between the  
460 catalytic histidine and serine (53). The chemical similarity of the D-OH butenolide ring of karrikin  
461 and GR24 suggests that the KL signal may share a parallel structure and perhaps is biochemically  
462 processed via multiple steps and intermediate adducts. Therefore, the significance of this finding  
463 may also shed light on SL perception and cleavage by D14, which are still elusive. While the MS  
464 data corroborate a mass shift corresponding to an intermediate covalently bound to KAI2s, the  
465 adduct was detected more significantly on the catalytic histidine rather than on the serine. This  
466 data is in agreement with the expected transient nature of the serine nucleophilic attack, and the  
467 more stable adduct that can be formed on the catalytic histidine. Collectively, the crystal structure  
468 of PsKAI2B bound to enantiomeric SL synthetic analog and the MS data reveal, for the first time,  
469 the mode of action of KAI2 not only as receptors but also as bona fide enzymes. Beyond the  
470 importance of illuminating the stereoselectivity of ligand perception diverged KAI2 receptors in  
471 KAR/KL signaling pathways, our data strongly suggest the through the evolution of KAI2  
472 enzymes, specific structural and functional adaptation diverged to enable more extended  
473 sensitivities to KAR/KL and SL and SL-like molecules by KAI2B.

474 Here, we elucidate the molecular basis for functional divergence of KAI2 receptors, focusing  
475 on a pea as model legume. Because of their ability to fix atmospheric nitrogen through plant–  
476 rhizobium symbiosis, legume crops such as pea or fava bean are attracting increasing attention for  
477 their agroecological potential. Thus, better understanding of KAR/KL perception and signaling in  
478 these key crops may have far-reaching impacts on agro-systems and food security.

479

480

## 481 **Methods**

482

### 483 *Protein sequence alignment and phylogenetic tree analyses*

484 Representative KAI2 sequences of 41 amino acid sequences were downloaded from Phytozome  
485 and specific genome databases as shown in **Fig. S1**. Alignment was performed in MEGA X (58)  
486 using the MUSCLE multiple sequence alignment algorithm (59). Sequence alignment graphics  
487 were generated using CLC Genomics Workbench v12. The evolutionary history was inferred by  
488 using the Maximum Likelihood method and JTT matrix-based model (60). Initial tree(s) for the  
489 heuristic search were obtained automatically by applying Neighbor-Join and BioNJ algorithms to  
490 a matrix of pairwise distances estimated using the JTT model, and then selecting the topology with  
491 superior log likelihood value. The percentage of trees in which the associated taxa clustered  
492 together is shown next to the branches (61). Tree is drawn to scale, with branch lengths measured  
493 in the number of substitutions per site. Analysis involved 41 amino acid sequences with a total of  
494 327 positions in the final dataset. Evolutionary analyses were conducted in MEGA X (58).

### 495 *RT-PCR analyses*

496 For PsKAI2A splicing variant detection, PCR reactions were performed using 1 µl of cDNA or  
497 genomic DNA sample in a final reaction mixture (20 µl) containing 2 µl of 10 x PCR buffer  
498 (ThermoFisher Scientific), 0.25 µL of 25 mM dNTPs, 0.25 µl of each primer at 10µM, and 1 unit

499 of Dream Taq DNA polymerase (ThermoFisher Scientific). Primer sequences are indicated in  
500 **Table S3**. PCR was performed in the following conditions: 94 °C/5 min, 94 °C/30 s, 58 °C/30 s,  
501 72 °C/1 min for 30 cycles. Half of each PCR product was loaded onto Ethidium bromide  
502 stained 1% agarose gels in TAE buffer, stained with ethidium bromide, and photographed with  
503 Molecular Imager<sup>®</sup> Gel Doc<sup>™</sup> XR System (BioRad)

504

### 505 *Constructs and generation of transgenic lines*

506 The expression vectors for transgenic Arabidopsis were constructed by MultiSite Gateway Three-  
507 Fragment Vector Construction kit (Invitrogen). *AtKAI2* and *PsKAI2A.2* constructs were tagged  
508 with 6xHA epitope tag, mCitrine protein or GUS protein at their C-terminus. Lines were resistant  
509 to hygromycin. The *AtKAI2* native promoter (0.7 kb) was cloned into the pDONR-P4P1R vector,  
510 using Gateway recombination (Invitrogen) as described in (62). The 6xHA with linker and  
511 mCitrine tags were cloned into pDONR-P2RP3 (Invitrogen) as described in de Saint Germain et  
512 al. (48). *PsKAI2A.1*, *PsKAI2A.2* and *PsKAI2B* CDS were PCR amplified from *Pisum* cv. Tèrese  
513 cDNA with the primers specified in **Table S3**. and then recombined into the pDONR221 vector  
514 (Invitrogen). The suitable combination of *AtKAI2* native promoter, *AtKAI2*, *PsKAI2A.1*,  
515 *PsKAI2A.2* or *PsKAI2B* and 6XHA, mCitrine or GUS was cloned into the pH7m34GW final  
516 destination vectors by using the three fragment recombination system (63) and were thusly named  
517 proAtKAI2:AtKAI2-6xHA, proAtKAI2:AtKAI2-mcitrine, proAtKAI2:AtKAI2-GUS,  
518 proAtKAI2:PsKAI2A.1-6xHA, proAtKAI2:PsKAI2A.2-mcitrine, proAtKAI2:PsKAI2A.2-GUS,  
519 proAtKAI2:PsKAI2B-6XHA, proAtKAI2:PsKAI2B-GUS and proAtKAI2:PsKAI2B-mcitrine..  
520 Transformation of Arabidopsis *htl-3* or *kai2-2* mutant was performed according to the  
521 conventional floral dipping method (64), with Agrobacterium strain GV3101. For each construct,

522 only a few independent T1 lines were isolated, and all lines were selected in T2. Phenotypic  
523 analysis shown in **Fig. 1e** was performed on the T3 homozygous lines.

524

#### 525 ***Protein extraction and immunoblotting.***

526 Total protein extract was prepared from 8 to 10, 10 day-old Arabidopsis seedling in Laemmli  
527 buffer and boiled for 5 min. Total protein were separated by 10% SDS-PAGE and transferred onto  
528 polyvinylidene difluoride membrane (Bio-Rad) probed with anti-HA primary antibody (1:10000;  
529 SIGMA H9658-100UL Lot#128M4789V) and then anti-mouse-IgG-HRP secondary antibody  
530 (1:10000; SIGMA A9044-2ML-100UL Lot#029M4799V) or with anti-GFP primary antibody  
531 (1:10000; CHROMTEK 3H9-100 Lot#60706001AB) and then anti-rat-IgG-HRP secondary  
532 antibody (1:10000; SIGMA A9037-1ML Lot#SLCF6775). Ponceau staining was used as a loading  
533 control.

534

#### 535 ***Identification of Pskai2a and Pskai2b Targeting-Induced Local Lesions IN Genomes***

##### 536 ***(TILLING) mutants***

537 The mutagenized population in the pea cultivar (cv.) Caméor was used as a TILLING resource.  
538 For obtaining mutants in *PsKAI2A*, TILLING analysis was performed on 5000 families within one  
539 amplicon of 1068 bp using nested primers (N1, N2) with PsKAI2A\_N1F primer and  
540 PsKAI2A\_N1R primer PsKAI2A\_N2Ftag primer and PsKAI2A\_N2Rtag primer Primers are  
541 indicated in **Table S3**. The enzymatic mutation detection technique based on the mismatch specific  
542 endonuclease ENDO1 was used. For *PsKAI2B*, the mutation detection system by sequencing and  
543 described in (65) was used. Two amplicons of 381 and 401 bp were screened in 2500 families.  
544 Primers are indicated in **Table S3**. Prediction of the amino acid changes that affect protein function  
545 was made using the SIFT program ([sift.jcvi.org/](http://sift.jcvi.org/)).



546 M3 and M4 seeds from lines carrying mutations in the *PsKAI2A* and *PsKAI2B* genes were  
547 genotyped for homozygous mutant plants; these plants were backcrossed once (alleles *Pskai2a-4*,  
548 *Pskai2b-1*, *Pskai2b-2*) to three or four times (alleles *Pskai2a-2*, *Pskai2a-6*, *Pskai2b-3*) to the cv.  
549 Caméor. BC1-F3 and M5 single mutant plants were crossed for obtaining the *Pskai2a-6 Pskai2b-*  
550 *3* double mutant.

551

### 552 ***Plant material and growth conditions.***

553 For branching quantification, *Pisum sativum* plants were grown in glasshouse (23°C day/ 15°C  
554 night) under a 16-h photoperiod (the natural daylength was extended or supplemented during the  
555 day when necessary using sodium lamps) in pots filled with clay pellets, peat, and soil (1:1:1)  
556 supplied regularly with nutrient solution. Nodes were numbered acropetally from the first scale  
557 leaf as node 1.

558

### 559 ***Root hair assay***

560 *Pisum sativum* *Cameor* wild-type, *Pskai2a-3*, *Pskai2b-6*, *Pskai2a-3 Pskai2a-6* seeds were surface  
561 sterilized with 1% NaClO, washed 5 times, and incubated for 2 hours in sterile water. Imbibed  
562 seeds were germinated on ½ MS, pH 5.8 containing 1% agar at 4°C for 3 days in the dark.  
563 Seedlings were grown in axenic conditions on 12x12 cm square Petri dishes at 24°C with 16-h-  
564 light/8-h-dark cycles. To assess root hair length, images of the primary root tips of 10-day old  
565 seedlings were taken with a Zeiss Discovery V8 microscope equipped with a Zeiss Axiocam 503  
566 camera. Root hair length was measured for a minimum of 8 roots per genotype for 8 different root  
567 hairs per root, between 10 and 20 mm from the root tip using Fiji as described (66). For root-hair  
568 length measurements a Welch t-test, p-value < 0.05 and for RT-qPCR analysis a Kruskal-Wallis

569 Test with post-hoc Student's t-test,  $p < 0.05$  were performed using R statistical environment  
570 (<https://www.r-project.org/>). For the Kruskal-Wallis Test the R-package agricolae  
571 (<https://CRAN.R-project.org/package=agricolae>) was used.

572

### 573 *Treatment for analysis of transcript accumulation*

574 For treatments with KARs and GR24 enantiomers, 10-day old seedlings grown on Petri dishes as  
575 described above, were placed with their roots into 50 ml amber Falcon tubes filled with ½ MS  
576 solution for 24 h to allow the seedlings to adapt to the new growth system. For the treatment the  
577 growth media was exchanged with ½ MS solution containing 3µM Karrikin<sub>1</sub>, Karrikin<sub>2</sub>,  
578 ([www.olchemim.cz](http://www.olchemim.cz)), (+)-GR24 or (-)-GR24 ([www.strigolab.eu](http://www.strigolab.eu)) and seedlings were incubated  
579 with their shoots in the light for 4 hours.

### 580 *Analysis of transcript accumulation by RT-qPCR*

581 For analysis of transcript levels by RT-qPCR presented in figure 1, total RNA was isolated from  
582 28 days old plant for flower and flower bud and from 10 days old plants for all other tissues, using  
583 TRIZOL reagent (Invitrogen) following the manufacturer's protocol. DNase treatment was  
584 performed to remove DNA using the Qiagen RNase-Free DNase Set (79254) and the RNeasy Mini  
585 Kit (74904) and eluted in 50 mL of RNase-free water. RNA was quantified using NanoDrop 1000  
586 and migrated on gels to check RNA non-degradation. Total cDNA was synthesized from 2 mg of  
587 total RNA using 50 units of RevertAid H Moloney murine leukemia virus reverse transcriptase in  
588 30 µL following the manufacturer's instructions with poly(T)<sub>18</sub> primer. cDNA was diluted 10  
589 times before subsequent analysis. Quantitative reverse transcription-PCR analyses were adapted  
590 from (67). They were performed using SsoAdvanced™ Universal SYBR® Green SuperMix  
591 (Biorad). Cycling conditions for amplification were 95°C for 10 min, 50 cycles of 95°C for 5 s,

592 62°C for 5 s, and 72°C for 15 s, followed by 0.1°C s<sup>-1</sup> ramping up to 95°C for fusion curve  
593 characterization. Two biological repeats were analyzed in duplicate. To calculate relative transcript  
594 levels, the comparative cycle method based on non-equal efficiencies was used (68). Transcript  
595 levels for the different genes were expressed relative to the expression of the *PsACTIN* gene.  
596 Primers are indicated in **Table S3**.

597 For analysis of transcript levels by RT-qPCR presented in **Fig. 2**, plant tissue was rapidly shock  
598 frozen in liquid nitrogen and ground to a fine powder with a mortar and pestle. RNA was extracted  
599 using the Spectrum Plant Total RNA Kit (www.sigmaaldrich.com). The RNA was treated with  
600 Invitrogen DNase I amp. grade (www.invitrogen.com) and tested for purity by PCR. cDNA  
601 synthesis was performed with 1 µg RNA using the iScript cDNA Synthesis kit (www.Biorad.com).  
602 cDNA was diluted in water in a 1:10 ratio and 1µl was used for RT-PCR was performed with an  
603 iCycler (Biorad, www.bio-rad.com/) using a Green MasterMix (Jena Bioscience, highROX, 2x  
604 conc.). Thermal cycler conditions were: 95°C 2 min, 45 cycles of 95°C 30 sec, 60°C 30sec and  
605 72°C 20 sec followed by dissociation curve analysis. Expression levels were calculated according  
606 to the  $\Delta\Delta C_t$  method (69). For each genotype and treatment three to four biological replicates were  
607 monitored and each sample was represented by two technical replicates. Transcript levels for the  
608 different genes were expressed relative to the expression of the *PsTUB* gene, Accession:X54844,  
609 (70). Primers are indicated in **Table S3**.

610

### 611 ***Hypocotyl elongation assays.***

612 Arabidopsis seeds were surface sterilized by consecutive treatments of 5 min 70% (v/v) ethanol  
613 with 0.05% (w/v) sodium dodecyl sulfate (SDS) and 5 min 95% (v/v) ethanol. Then seeds were  
614 sown on half-strength Murashige and Skoog (½ MS) media (Duchefa Biochemie) containing 1%

615 agar, supplemented with 1  $\mu$ M (-)-GR24 or with 0.01 % DMSO (control). Seeds were stratified at  
616 4 °C (2 days in dark) then transferred to the growth chamber at 22 °C, under 20-30  $\mu$ E /m<sup>2</sup>/sec of  
617 white light in long day conditions (16 hr light/ 8 hr dark). Seedlings were photographed and  
618 hypocotyl lengths were quantified using ImageJ (71). 2 plates of 10-12 seeds were sown for each  
619 genotype x treatment. Using Student t-tests, no statistically significantly different means were  
620 detected between plates. The data from the 20-24 seedlings were then used for a one-way ANOVA.

621

### 622 *Chemicals*

623 Enantiopure GR24 isomers were obtained as described in de Saint Germain et al. (48) or purchased  
624 from StrigoLab. Karrikin<sub>1</sub> and Karrikin<sub>2</sub> were purchased from Olchemim. Profluorescent probes  
625 (GC240, GC486) were obtained as described in de Saint Germain et al. (48, 72).

626

### 627 *Protein preparation and purification*

628 PsKAI2A.2, PsKAI2B, and all described mutants were independently cloned and expressed as a  
629 6 $\times$  His-SUMO fusion proteins from the expression vector pAL (Addgene). These were cloned  
630 utilizing primers in **Table S3**. BL21 (DE3) cells transformed with the expression plasmid were  
631 grown in LB broth at 16 °C to an OD<sub>600</sub> of ~0.8 and induced with 0.2 mM IPTG for 16 h. Cells  
632 were harvested, re-suspended and lysed in extract buffer (50 mM Tris, pH 8.0, 200 mM NaCl, 5  
633 mM imidazole, 4% Glycerol). All His-SUMO-PsKAI2s were isolated from soluble cell lysate by  
634 Ni-NTA resin. The His-SUMO-PsKAI2 was eluted with 250 mM imidazole and subjected to  
635 anion-exchange. The eluted protein was then cleaved with TEV (tobacco etch virus) protease  
636 overnight at 4 °C. The cleaved His-SUMO tag was removed by passing through a Nickel  
637 Sepharose and PsKAI2 was further purified by chromatography through a Superdex-200 gel

638 filtration column in 20 mM HEPES, pH 7.2, 150 mM NaCl, 5 mM DTT, 1% Glycerol. All proteins  
639 were concentrated by ultrafiltration to 3–10 mg/mL<sup>-1</sup>. RMS3, AtD14, AtKAI2 were expressed in  
640 bacteria with TEV cleavable GST tag, purified and used as described in de Saint Germain et al.  
641 (48).

642

#### 643 *Enzymatic hydrolysis of GR24 isomers by purified proteins*

644 Ligands (10 μM) were incubated without and with purified proteins (5 μM) for 150 min at 25 °C  
645 in PBS (0.1 mL, pH 6.8) in presence of (±)-1-indanol (100 μM) as the internal standard. The  
646 solutions were acidified to pH 1 with 10% trifluoroacetic acid in CH<sub>3</sub>CN (v/v) (2 μL) to quench  
647 the reaction and centrifuged (12 min, 12,000 tr/min). Thereafter the samples were subjected to RP-  
648 UPLC-MS analyses using Ultra Performance Liquid Chromatography system equipped with a  
649 PDA and a Triple Quadrupole mass spectrometer Detector (Acquity UPLC-TQD, Waters, USA).  
650 RP-UPLC (HSS C<sub>18</sub> column, 1.8 μm, 2.1 mm × 50 mm) with 0.1% formic acid in CH<sub>3</sub>CN and  
651 0.1% formic acid in water (aq. FA, 0.1%, v/v, pH 2.8) as eluents [10% CH<sub>3</sub>CN, followed by linear  
652 gradient from 10 to 100% of CH<sub>3</sub>CN (4 min)] was carried out at a flow rate of 0.6 mL/min. The  
653 detection was performed by PDA using the TQD mass spectrometer operated in Electrospray  
654 ionization positive mode at 3.2 kV capillary voltage. The cone voltage and collision energy were  
655 optimized to maximize the signal and were respectively 20 V for cone voltage and 12 eV for  
656 collision energy and the collision gas used was argon at a pressure maintained near 4.5.10<sup>-3</sup> mBar.

657

#### 658 *Enzymatic assay with pro-fluorescent probes*

659 Enzymatic assay and analysis have been carried out as described in de Saint Germain et al. (48),  
660 using a TriStar LB 941 Multimode Microplate Reader from Berthold Technologies. The  
661 experiments were repeated three times.

662

### 663 *Protein melting temperatures*

664 Differential Scanning Fluorimetry (DSF) experiments were performed on a CFX96 Touch™  
665 Real-Time PCR Detection System (Bio-Rad Laboratories, Inc., Hercules, California, USA) using  
666 excitation and emission wavelengths of 490 and 575 nm, respectively. Sypro Orange ( $\lambda_{ex}/\lambda_{em}$  :  
667 470/570 nm; Life Technologies Co., Carlsbad, California, USA) was used as the reporter dye.  
668 Samples were heat-denatured using a linear 25 to 95 °C gradient at a rate of 1.3 °C per minute  
669 after incubation at 25 °C for 30 min in the absence of light. The denaturation curve was obtained  
670 using CFX manager™ software. Final reaction mixtures were prepared in triplicate in 96-well  
671 white microplates, and each reaction was carried out in 20  $\mu$ L scale in Phosphate buffer saline  
672 (PBS) (100 mM Phosphate, pH 6.8, 150 mM NaCl) containing 6  $\mu$ g protein (such that final  
673 reactions contained 10  $\mu$ M protein), 0-1000  $\mu$ M ligand (as shown on the **Fig. 4c-f** and **Fig. S8b-**  
674 **e**), 4% (v/v) DMSO, and 0.008  $\mu$ L Sypro Orange. Plates were incubated in darkness for 30 minutes  
675 before analysis. In the control reaction, DMSO was added instead of ligand. All experiments were  
676 repeated three times.

677

### 678 *Intrinsic tryptophan fluorescence assays and kinetics*

679 Intrinsic tryptophan fluorescence assays and determination of the dissociation constant  $K_D$  has  
680 been performed as described in de Saint Germain et al. (48), using the Spark® Multimode  
681 Microplate Reader from Tecan.

682 ***Crystallization, data collection and structure determination***

683 The crystals of PsKAI2B were grown at 25 °C by the hanging-drop vapor diffusion method with  
684 1.0 µL purified protein sample mixed with an equal volume of reservoir solution containing 0.1 M  
685 HEPES pH 7.5, 2.75% PEG 2000, 2.75% v/v PEG 3350, 2.75% v/v PEG 4000, 2.75% v/v PEG-  
686 ME 5000. The crystals of PsKAI2B in complex with (-)-GR24 were grown at 25 °C by the  
687 hanging-drop vapor diffusion method with 1.0 µL purified protein complex (preincubated with 1  
688 mM (-)-GR24, StrigoLab) and mixed with an equal volume of reservoir solution containing 0.1  
689 M HEPES pH 7.5, 2.75% PEG 2000, 2.75% v/v PEG 3350, 2.75% V/V PEG 4000, 2.75% v/v  
690 PEG-ME 5000, 1 mM (-)-GR24. Crystals of maximum size were obtained and harvested after 2  
691 weeks from the reservoir solution with additional 20% MPD serving as cryoprotectant. X-ray  
692 diffraction data was integrated and scaled with HKL2000 package (73). PsKAI2s crystal structures  
693 were determined by molecular replacement using the AtKAI2 model (PDB: 5Z9H) (74) as the  
694 search model. All structural models were manually built, refined, and rebuilt with PHENIX (75)  
695 and COOT (76).

696

697 ***Structural biology modelling and analyses***

698 Model structure illustrations were made by PyMOL (77). PsKAI2A model structure was generated  
699 using iTASSER (78). Ligand identification, ligand-binding pocket analyses, and computing  
700 solvent accessible surface values analyses were carried out using Phenix LigandFit (75), CASTp  
701 software (79), and AutoDock Vina (80), respectively. LigPlot+ program (81) was used for 2-D  
702 representation of protein-ligand interactions from standard PDB data format.

703

704 *Direct electrospray ionization – mass spectrometry of PsKAI2 proteins (ESI)-MS under*  
705 *denaturing conditions*

706 Mass spectrometry measurements were performed with an electrospray Q-TOF mass spectrometer  
707 (Waters) equipped with the Nanomate device (Advion, Inc.). The HD\_A\_384 chip (5  $\mu\text{m}$  I.D.  
708 nozzle chip, flow rate range 100–500 nL/min) was calibrated before use. For ESI–MS  
709 measurements, the Q-TOF instrument was operated in RF quadrupole mode with the TOF data  
710 being collected between  $m/z$  400–2990. Collision energy was set to 10 eV and argon was used as  
711 the collision gas. PsKAI2 proteins (50  $\mu\text{M}$ ) in 50 mM ammonium acetate (pH 6.8) in presence or  
712 without (-)-GR24 (500  $\mu\text{M}$ ) were incubated for 10 min at room temperature before denaturation  
713 in 50% acetonitrile and 1% formic acid. The solutions were directly injected for Mass spectra  
714 acquisition or digested before LC-MS/MS analyses. Mass Lynx version 4.1 (Waters) and  
715 Peakview version 2.2 (Sciex) software were used for acquisition and data processing, respectively.  
716 Deconvolution of multiply charged ions was performed by applying the MaxEnt algorithm (Sciex).  
717 The average protein masses were annotated in the spectra and the estimated mass accuracy was  $\pm$   
718 2 Da. External calibration was performed with NaI clusters (2  $\mu\text{g}/\mu\text{L}$ , isopropanol/H<sub>2</sub>O 50/50,  
719 Waters) in the acquisition  $m/z$  mass range.

720  
721 **Acknowledgements:** N.S. is supported by NSF-CAREER (Award #2047396) and NSF-EAGER  
722 (Award #2028283). This work is also supported by the CHARM3AT Labex program (ANR-11-  
723 LABX-39) to F.-D.B.; by AgreenSkills from the European Union in the framework of the Marie-  
724 Curie FP7 COFUND People Programme and a fellowship from Saclay Plant Sciences (ANR-17-  
725 EUR-0007) to A.d.S.G.; and by the Emmy Noether program (GU1423/1-1) of the Deutsche  
726 Forschungsgemeinschaft (DFG) to C.G.. Furthermore, this work was supported by the Institut  
727 Jean-Pierre Bourgin's Plant Observatory technological platforms. We thank the beamline staff at



728 the Advanced Light Source (U.S. DOE Office of Science User Facility under Contract No. DE-  
729 AC02-05CH11231, is supported in part by the ALS-ENABLE program funded by the National  
730 Institutes of Health, National Institute of General Medical Sciences, grant P30 GM124169-01).  
731 We thank the facilities and expertise of the I2BC proteomic platform (Proteomic-Gif, SICaPS)  
732 supported by IBiSA, Ile de France Region, Plan Cancer, CNRS and Paris-Sud University

733  
734 **Author Contributions:** AM.G., S.T., F.-D.B., C.R., C.G., A.dS.G., and N.S. conceived and  
735 designed the experiments. N.S., A.dS.G., and AM.G. conducted the protein purification,  
736 biochemical and crystallization experiments. J.-P.P. characterized pea Tilling mutants. S.T.  
737 performed pea RT-qPCR and root hair assay. P.LB. obtained Arabidopsis complementation lines.  
738 A.B., M.D. and C.LS. generated pea TILLING mutant collection. D.C. performed the mass  
739 experiments. N.S. and AM.G. determined and analyzed crystal structures and conducted in silico  
740 studies. S. T. performed pea root hair assays and gene expression analysis in **Fig. 2**. AM.G.,  
741 A.dS.G., and N.S. wrote the manuscript with help from S.T., F.-D.B., C.R. and C.G..

742 **Disclosure Statement:** N.S. has an equity interest in Oerth Bio and serves on the company's  
743 Scientific Advisory Board.

744 **Data and materials availability:**

745 The atomic coordinates of apo and ligand-bound forms of PsKAI2 structures has been deposited  
746 in the Protein Data Bank with accession codes 7K2Z and 7K38, respectively. All relevant data are  
747 available from corresponding authors upon request.

748

749 **References**

- 750 1. G. R. Flematti, E. L. Ghisalberti, K. W. Dixon, R. D. Trengove, A compound from smoke  
751 that promotes seed germination. *Science*. **305**, 977 (2004).
- 752 2. G. R. Flematti, E. D. Goddard-Borger, D. J. Merritt, E. L. Ghisalberti, K. W. Dixon, R. D.  
753 Trengove, Preparation of 2H-furo[2,3-c]pyran-2-one derivatives and evaluation of their  
754 germination-promoting activity. *J. Agric. Food Chem.* **55**, 2189–2194 (2007).
- 755 3. G. R. Flematti, A. Scaffidi, K. W. Dixon, S. M. Smith, E. L. Ghisalberti, Production of the  
756 seed germination stimulant karrikinolide from combustion of simple carbohydrates. *J.*  
757 *Agric. Food Chem.* **59**, 1195–1198 (2011).
- 758 4. K. W. Dixon, D. J. Merritt, G. R. Flematti, E. L. Ghisalberti, Karrikinolide - A  
759 phytoreactive compound derived from smoke with applications in horticulture, ecological  
760 restoration and agriculture. *Acta Hortic.* **813** (2009).
- 761 5. J. C. Stevens, D. J. Merritt, G. R. Flematti, E. L. Ghisalberti, K. W. Dixon, Seed  
762 germination of agricultural weeds is promoted by the butenolide 3-methyl-2H-furo[2,3-  
763 c]pyran-2-one under laboratory and field conditions. *Plant Soil.* **298**, 113–124 (2007).
- 764 6. R. L. Long, K. Williams, E. M. Griffiths, G. R. Flematti, D. J. Merritt, J. C. Stevens, S. R.  
765 Turner, S. B. Powles, K. W. Dixon, Prior hydration of Brassica tournefortii seeds reduces  
766 the stimulatory effect of karrikinolide on germination and increases seed sensitivity to  
767 abscisic acid. *Ann. Bot.* **105**, 1063–1070 (2010).
- 768 7. D. C. Nelson, A. Scaffidi, E. A. Dun, M. T. Waters, G. R. Flematti, K. W. Dixon, C. A.  
769 Beveridge, E. L. Ghisalberti, S. M. Smith, F-box protein MAX2 has dual roles in karrikin  
770 and strigolactone signaling in Arabidopsis thaliana. *Proc. Natl. Acad. Sci.* **108**, 8897–8902  
771 (2011).
- 772 8. M. T. Waters, D. C. Nelson, A. Scaffidi, G. R. Flematti, Y. K. Sun, K. W. Dixon, S. M.  
773 Smith, Specialisation within the DWARF14 protein family confers distinct responses to  
774 karrikins and strigolactones in Arabidopsis. *Development.* **139**, 1285–1295 (2012).
- 775 9. Y. Guo, Z. Zheng, J. J. La Clair, J. Chory, J. P. Noel, Smoke-derived karrikin perception  
776 by the  $\alpha/\beta$  hydrolase KAI2 from Arabidopsis. *Proc. Natl. Acad. Sci.* **110**, 8284–8289  
777 (2013).
- 778 10. M. Kagiya, Y. Hirano, T. Mori, S. Y. Kim, J. Kyojuka, Y. Seto, S. Yamaguchi, T.  
779 Hakoshima, Structures of D14 and D14L in the strigolactone and karrikin signaling  
780 pathways. *Genes to Cells.* **18**, 147–160 (2013).
- 781 11. J. P. Stanga, S. M. Smith, W. R. Briggs, D. C. Nelson, SUPPRESSOR OF MORE  
782 AXILLARY GROWTH2 1 Controls Seed Germination and Seedling Development in  
783 Arabidopsis. *Plant Physiol.* **163**, 318–330 (2013).
- 784 12. D. C. Nelson, G. R. Flematti, J. A. Riseborough, E. L. Ghisalberti, K. W. Dixon, S. M.  
785 Smith, Karrikins enhance light responses during germination and seedling development  
786 in Arabidopsis thaliana. *Proc. Natl. Acad. Sci. U. S. A.* **107**, 7095–7100 (2010).
- 787 13. X. D. Sun, M. Ni, HYPOSENSITIVE to LIGHT, an  $\alpha/\beta$  fold protein, acts  
788 downstream of ELONGATED HYPOCOTYL 5 to regulate seedling de-etiolation. *Mol.*  
789 *Plant.* **4**, 116–126 (2011).

- 790 14. J. Yao, M. T. Waters, Perception of karrikins by plants: A continuing enigma. *J. Exp. Bot.*  
791 **71**, 1774-1781 (2020).
- 792 15. M. T. Waters, A. Scaffidi, Y. K. Sun, G. R. Flematti, S. M. Smith, The karrikin response  
793 system of Arabidopsis. *Plant J.* **79**, 623–631 (2014).
- 794 16. C. Gutjahr, E. Gobbato, J. Choi, M. Riemann, M. G. Johnston, W. Summers, S.  
795 Carbonnel, C. Mansfield, S. Y. Yang, M. Nadal, I. Acosta, M. Takano, W. B. Jiao, K.  
796 Schneeberger, K. A. Kelly, U. Paszkowski, Rice perception of symbiotic arbuscular  
797 mycorrhizal fungi requires the karrikin receptor complex. *Science.* **350**, 1521–1524  
798 (2015).
- 799 17. W. Li, K. H. Nguyen, H. D. Chu, C. Van Ha, Y. Watanabe, Y. Osakabe, M. A. Leyva-  
800 González, M. Sato, K. Toyooka, L. Voges, M. Tanaka, M. G. Mostofa, M. Seki, M. Seo,  
801 S. Yamaguchi, D. C. Nelson, C. Tian, L. Herrera-Estrella, L. S. P. Tran, The karrikin  
802 receptor KAI2 promotes drought resistance in Arabidopsis thaliana. *PLoS Genet.* **13**,  
803 e1007076 (2017).
- 804 18. L. Wang, M. T. Waters, S. M. Smith, Karrikin-KAI2 signalling provides Arabidopsis  
805 seeds with tolerance to abiotic stress and inhibits germination under conditions  
806 unfavourable to seedling establishment. *New Phytol.* **219**, 605–618 (2018).
- 807 19. A. Scaffidi, M. T. Waters, C. S. Bond, K. W. Dixon, S. M. Smith, E. L. Ghisalberti, G. R.  
808 Flematti, Exploring the molecular mechanism of karrikins and strigolactones. *Bioorganic*  
809 *Med. Chem. Lett.* **22**, 3743–3746 (2012).
- 810 20. K. Yoneyama, Recent progress in the chemistry and biochemistry of strigolactones. *J.*  
811 *Pestic. Sci.* **45**, 45–53 (2020).
- 812 21. L. H. Zhao, X. Edward Zhou, Z. S. Wu, W. Yi, Y. Xu, S. Li, T. H. Xu, Y. Liu, R. Z. Chen,  
813 A. Kovach, Y. Kang, L. Hou, Y. He, C. Xie, W. Song, D. Zhong, Y. Xu, Y. Wang, J. Li,  
814 C. Zhang, K. Melcher, H. Eric Xu, Crystal structures of two phytohormone signal-  
815 transducing  $\alpha/\beta$  hydrolases: Karrikin-signaling KAI2 and strigolactone-signaling  
816 DWARF14. *Cell Res.* **23**, 436–439 (2013).
- 817 22. K. Akiyama, K. I. Matsuzaki, H. Hayashi, Plant sesquiterpenes induce hyphal branching  
818 in arbuscular mycorrhizal fungi. *Nature.* **435**, 824–827 (2005).
- 819 23. V. Gomez-Roldan, S. Fermas, P. B. Brewer, V. Puech-Pagès, E. A. Dun, J. P. Pillot, F.  
820 Letisse, R. Matusova, S. Danoun, J. C. Portais, H. Bouwmeester, G. Bécard, C. A.  
821 Beveridge, C. Rameau, S. F. Rochange, Strigolactone inhibition of shoot branching.  
822 *Nature.* **455**, 189–194 (2008).
- 823 24. J. Agusti, S. Herold, M. Schwarz, P. Sanchez, K. Ljung, E. A. Dun, P. B. Brewer, C. A.  
824 Beveridge, T. Sieberer, E. M. Sehr, T. Greb, Strigolactone signaling is required for auxin-  
825 dependent stimulation of secondary growth in plants. *Proc. Natl. Acad. Sci. U. S. A.* **180**,  
826 20242–20247 (2011).
- 827 25. Y. Kapulnik, P. M. Delaux, N. Resnick, E. Mayzlish-Gati, S. Wininger, C. Bhattacharya,  
828 N. Séjalon-Delmas, J. P. Combier, G. Bécard, E. Belausov, T. Beeckman, E. Dor, J.  
829 Hershenhorn, H. Koltai, Strigolactones affect lateral root formation and root-hair  
830 elongation in Arabidopsis. *Planta.* **233**, 209–216 (2011).

- 831 26. A. Rasmussen, M. G. Mason, C. de Cuyper, P. B. Brewer, S. Herold, J. Agusti, D. Geelen,  
832 T. Greb, S. Goormachtig, T. Beeckman, C. A. Beveridge, Strigolactones suppress  
833 adventitious rooting in arabidopsis and pea. *Plant Physiol.* **158**, 1976–1987 (2012).
- 834 27. M. T. Waters, C. Gutjahr, T. Bennett, D. C. Nelson, Strigolactone Signaling and  
835 Evolution. *Annu. Rev. Plant Biol.* **68**, 291–322 (2017).
- 836 28. C. E. Cook, L. P. Whichard, B. Turner, M. E. Wall, G. H. Egley, Germination of  
837 witchweed (*striga lutea* Lour.): Isolation and properties of a potent stimulant. *Science.* **154**,  
838 1189–1190 (1966).
- 839 29. R. Bythell-Douglas, C. J. Rothfels, D. W. D. Stevenson, S. W. Graham, G. K. S. Wong,  
840 D. C. Nelson, T. Bennett, Evolution of strigolactone receptors by gradual neo-  
841 functionalization of KAI2 paralogues. *BMC Biol.* **15**, 1–21 (2017).
- 842 30. S. M. Swarbreck, Y. Guerringue, E. Matthus, F. J. C. Jamieson, J. M. Davies, Impairment  
843 in karrikin but not strigolactone sensing enhances root skewing in *Arabidopsis thaliana*.  
844 *Plant J.* **98**, 607–621 (2019).
- 845 31. S. Toh, D. Holbrook-Smith, P. J. Stogios, O. Onopriyenko, S. Lumba, Y. Tsuchiya, A.  
846 Savchenko, P. McCourt, Structure-function analysis identifies highly sensitive  
847 strigolactone receptors in *Striga*. *Science.* **350**, 203–207 (2015).
- 848 32. Y. Xu, T. Miyakawa, H. Nakamura, A. Nakamura, Y. Imamura, T. Asami, M. Tanokura,  
849 Structural basis of unique ligand specificity of KAI2-like protein from parasitic weed  
850 *Striga hermonthica*. *Sci. Rep.* **6**, 1–9 (2016).
- 851 33. M. T. Waters, A. Scaffidi, S. L. Y. Moulin, Y. K. Sun, G. R. Flematti, S. M. Smith, A  
852 selaginella moellendorffii ortholog of KARRIKIN INSENSITIVE2 functions in  
853 arabidopsis development but cannot mediate responses to karrikins or strigolactones.  
854 *Plant Cell.* **27**, 1925–1944 (2015).
- 855 34. M. Bürger, K. Mashiguchi, H. J. Lee, M. Nakano, K. Takemoto, Y. Seto, S. Yamaguchi, J.  
856 Chory, Structural Basis of Karrikin and Non-natural Strigolactone Perception in  
857 *Physcomitrella patens*. *Cell Rep.* **26**, 855–865 (2019).
- 858 35. Y. K. Sun, J. Yao, A. Scaffidi, K. T. Melville, S. F. Davies, C. S. Bond, S. M. Smith, G.  
859 R. Flematti, M. T. Waters, Divergent receptor proteins confer responses to different  
860 karrikins in two ephemeral weeds. *Nat. Commun.* **11** (2020), doi:10.1038/s41467-020-  
861 14991-w.
- 862 36. A. de Saint Germain, A. Jacobs, G. Brun, J. B. Pouvreau, L. Braem, D. Cornu, G. Clavé,  
863 E. Baudu, V. Steinmetz, V. Servajean, S. Wicke, K. Gevaert, P. Simier, S. Goormachtig,  
864 P. Delavault, F. D. Boyer, A Phelipanche ramosa KAI2 protein perceives strigolactones  
865 and isothiocyanates enzymatically. *Plant Commun.* (2021),  
866 doi:10.1016/j.xplc.2021.100166.
- 867 37. Y. K. Sun, G. R. Flematti, S. M. Smith, M. T. Waters, Reporter gene-facilitated detection  
868 of compounds in arabidopsis leaf extracts that activate the karrikin signaling pathway.  
869 *Front. Plant Sci.* **7**, 1799 (2016).
- 870 38. S. Carbonnel, S. Torabi, M. Griesmann, E. Bleek, Y. Tang, S. Buchka, V. Basso, M.  
871 Shindo, F. D. Boyer, T. L. Wang, M. Udvardi, M. T. Waters, C. Gutjahr, *Lotus japonicus*

- 872 karrikin receptors display divergent ligand-binding specificities and organ-dependent  
873 redundancy. *PLoS Genet.* **16**, e1009249 (2020).
- 874 39. C. E. Conn, D. C. Nelson, Evidence that KARRIKIN-INSENSITIVE2 (KAI2) Receptors  
875 may Perceive an Unknown Signal that is not Karrikin or Strigolactone. *Front. Plant Sci.* **6**,  
876 1–7 (2016).
- 877 40. C. Hamiaux, R. S. M. Drummond, B. J. Janssen, S. E. Ledger, J. M. Cooney, R. D.  
878 Newcomb, K. C. Snowden, DAD2 is an  $\alpha/\beta$  hydrolase likely to be involved in the  
879 perception of the plant branching hormone, strigolactone. *Curr. Biol.* **22**, 2032–2036  
880 (2012).
- 881 41. L. H. Zhao, X. E. Zhou, W. Yi, Z. Wu, Y. Liu, Y. Kang, L. Hou, P. W. De Waal, S. Li, Y.  
882 Jiang, A. Scaffidi, G. R. Flematti, S. M. Smith, V. Q. Lam, P. R. Griffin, Y. Wang, J. Li,  
883 K. Melcher, H. E. Xu, Destabilization of strigolactone receptor DWARF14 by binding of  
884 ligand and E3-ligase signaling effector DWARF3. *Cell Res.* **25**, 1219–1236 (2015).
- 885 42. Y. Xu, T. Miyakawa, S. Nosaki, A. Nakamura, Y. Lyu, H. Nakamura, U. Ohto, H. Ishida,  
886 T. Shimizu, T. Asami, M. Tanokura, Structural analysis of HTL and D14 proteins reveals  
887 the basis for ligand selectivity in *Striga*. *Nat. Commun.* **9**, 3947 (2018).
- 888 43. J. Kreplak, M. A. Madoui, P. Cápál, P. Novák, K. Labadie, G. Aubert, P. E. Bayer, K. K.  
889 Gali, R. A. Syme, D. Main, A. Klein, A. Bérard, I. Vrbová, C. Fournier, L. D’Agata, C.  
890 Belser, W. Berrabah, H. Toegelová, Z. Milec, J. Vrána, H. T. Lee, A. Kougbéadjo, M.  
891 Térézol, C. Huneau, C. J. Turo, N. Mohellibi, P. Neumann, M. Falque, K. Gallardo, R.  
892 McGee, B. Tar’an, A. Bendahmane, J. M. Aury, J. Batley, M. C. Le Paslier, N. Ellis, T. D.  
893 Warkentin, C. J. Coyne, J. Salse, D. Edwards, J. Lichtenzweig, J. Macas, J. Doležel, P.  
894 Wincker, J. Burstin, A reference genome for pea provides insight into legume genome  
895 evolution. *Nat. Genet.* **51**, 1411–1422 (2019).
- 896 44. K. Triques, B. Sturbois, S. Gallais, M. Dalmais, S. Chauvin, C. Clepet, S. Aubourg, C.  
897 Rameau, M. Caboche, A. Bendahmane, Characterization of *Arabidopsis thaliana*  
898 mismatch specific endonucleases: Application to mutation discovery by TILLING in pea.  
899 *Plant J.* **51** (2007), doi:10.1111/j.1365-313X.2007.03201.x.
- 900 45. M. Dalmais, J. Schmidt, C. Le Signor, F. Moussy, J. Burstin, V. Savoie, G. Aubert, V.  
901 Brunaud, Y. de Oliveira, C. Guichard, R. Thompson, A. Bendahmane, UTILdb, a *Pisum*  
902 *sativum* in silico forward and reverse genetics tool. *Genome Biol.* **9** (2008),  
903 doi:10.1186/gb-2008-9-2-r43.
- 904 46. J. A. Villacéjija-Aguilar, M. Hamon-Josse, S. Carbonnel, A. Kretschmar, C. Schmidt, C.  
905 Dawid, T. Bennett, C. Gutjahr, SMAX1/SMXL2 regulate root and root hair development  
906 downstream of KAI2-mediated signalling in *Arabidopsis*. *PLoS Genet.* (2019),  
907 doi:10.1371/journal.pgen.1008327.
- 908 47. A. Scaffidi, M. T. Waters, Y. K. Sun, B. W. Skelton, K. W. Dixon, E. L. Ghisalberti, G.  
909 R. Flematti, S. M. Smith, Strigolactone hormones and their stereoisomers signal through  
910 two related receptor proteins to induce different physiological responses in *Arabidopsis*.  
911 *Plant Physiol.* **165**, 1221–1232 (2014).
- 912 48. A. De Saint Germain, G. Clavé, M. A. Badet-Denisot, J. P. Pillot, D. Cornu, J. P. Le Caer,  
913 M. Burger, F. Pelissier, P. Retailleau, C. Turnbull, S. Bonhomme, J. Chory, C. Rameau, F.

- 914 D. Boyer, An histidine covalent receptor and butenolide complex mediates strigolactone  
915 perception. *Nat. Chem. Biol.* **12**, 787–794 (2016).
- 916 49. J. Yao, K. Mashiguchi, A. Scaffidi, T. Akatsu, K. T. Melville, R. Morita, Y. Morimoto, S.  
917 M. Smith, Y. Seto, G. R. Flematti, S. Yamaguchi, M. T. Waters, An allelic series at the  
918 KARRIKIN INSENSITIVE 2 locus of *Arabidopsis thaliana* decouples ligand hydrolysis  
919 and receptor degradation from downstream signalling. *Plant J.* **96**, 75–89 (2018).
- 920 50. R. Yao, F. Wang, Z. Ming, X. Du, L. Chen, Y. Wang, W. Zhang, H. Deng, D. Xie,  
921 ShHTL7 is a non-canonical receptor for strigolactones in root parasitic weeds. *Cell Res.*  
922 **27** (2017), , doi:10.1038/cr.2017.3.
- 923 51. R. Bythell-Douglas, M. T. Waters, A. Scaffidi, G. R. Flematti, S. M. Smith, C. S. Bond,  
924 The Structure of the Karrikin-Insensitive Protein (KAI2) in *Arabidopsis thaliana*. *PLoS*  
925 *One.* **8**, e54758 (2013).
- 926 52. Y. Seto, R. Yasui, H. Kameoka, M. Tamiru, M. Cao, R. Terauchi, A. Sakurada, R. Hirano,  
927 T. Kisugi, A. Hanada, M. Umehara, E. Seo, K. Akiyama, J. Burke, N. Takeda-Kamiya, W.  
928 Li, Y. Hirano, T. Hakoshima, K. Mashiguchi, J. P. Noel, J. Kyojuka, S. Yamaguchi,  
929 Strigolactone perception and deactivation by a hydrolase receptor DWARF14. *Nat.*  
930 *Commun.* **10**, 191 (2019).
- 931 53. R. Yao, Z. Ming, L. Yan, S. Li, F. Wang, S. Ma, C. Yu, M. Yang, L. Chen, L. Chen, Y.  
932 Li, C. Yan, D. Miao, Z. Sun, J. Yan, Y. Sun, L. Wang, J. Chu, S. Fan, W. He, H. Deng, F.  
933 Nan, J. Li, Z. Rao, Z. Lou, D. Xie, DWARF14 is a non-canonical hormone receptor for  
934 strigolactone. *Nature.* **536**, 469–473 (2016).
- 935 54. S. Carbonnel, D. Das, K. Varshney, M. C. Kolodziej, J. A. Villaécija-Aguilar, C. Gutjahr,  
936 The karrikin signaling regulator SMAX1 controls *Lotus japonicus* root and root hair  
937 development by suppressing ethylene biosynthesis. *Proc. Natl. Acad. Sci. U. S. A.* **117**  
938 (2020), doi:10.1073/pnas.2006111117.
- 939 55. C. E. Conn, R. Bythell-Douglas, D. Neumann, S. Yoshida, B. Whittington, J. H.  
940 Westwood, K. Shirasu, C. S. Bond, K. A. Dyer, D. C. Nelson, Convergent evolution of  
941 strigolactone perception enabled host detection in parasitic plants. *Science.* **349**, 540–543  
942 (2015).
- 943 56. J. K. Weng, M. Ye, B. Li, J. P. Noel, Co-evolution of Hormone Metabolism and Signaling  
944 Networks Expands Plant Adaptive Plasticity. *Cell.* **166**, 881–893 (2016).
- 945 57. H. Yoshida, E. Tanimoto, T. Hirai, Y. Miyanoiri, R. Mitani, M. Kawamura, M. Takeda, S.  
946 Takehara, K. Hirano, M. Kainosho, T. Akagi, M. Matsuoka, M. Ueguchi-Tanaka,  
947 Evolution and diversification of the plant gibberellin receptor GID1. *Proc. Natl. Acad. Sci.*  
948 *U. S. A.* **115**, E7844–E7853 (2018).
- 949 58. S. Kumar, G. Stecher, M. Li, C. Knyaz, K. Tamura, MEGA X: Molecular evolutionary  
950 genetics analysis across computing platforms. *Mol. Biol. Evol.* **35**, 1547–1549 (2018).
- 951 59. R. C. Edgar, MUSCLE: Multiple sequence alignment with high accuracy and high  
952 throughput. *Nucleic Acids Res.* **32**, 1792–1797 (2004).
- 953 60. D. T. Jones, W. R. Taylor, J. M. Thornton, The rapid generation of mutation data matrices  
954 from protein sequences. *Bioinformatics.* **8**, 275–282 (1992).

- 955 61. J. Felsenstein, Confidence Limits on Phylogenies: An Approach Using the Bootstrap.  
956 *Evolution (N. Y.)* **39**, 783–791 (1985).
- 957 62. M. Lopez-Obando, A. Guillory, F.-D. Boyer, D. Cornu, B. Hoffmann, P. Le Bris, J.-B.  
958 Pouvreau, P. Delavault, C. Rameau, A. de Saint Germain, S. Bonhomme, The  
959 Physcomitrium (Physcomitrella) patens PpKAI2L receptors for strigolactones and related  
960 compounds highlight MAX2 dependent and independent pathways. *bioRxiv* (2020).
- 961 63. M. Karimi, A. Bleys, R. Vanderhaeghen, P. Hilson, Building blocks for plant gene  
962 assembly. *Plant Physiol.* **145**, 1183–1191 (2007).
- 963 64. S. J. Clough, A. F. Bent, Floral dip: A simplified method for Agrobacterium-mediated  
964 transformation of Arabidopsis thaliana. *Plant J.* **16**, 735–743 (1998).
- 965 65. A. N. Kirienko, Y. B. Porozov, N. V. Malkov, G. A. Akhtemova, C. Le Signor, R.  
966 Thompson, C. Saffray, M. Dalmais, A. Bendahmane, I. A. Tikhonovich, E. A. Dolgikh,  
967 Role of a receptor-like kinase K1 in pea Rhizobium symbiosis development. *Planta.* **248**  
968 (2018), doi:10.1007/s00425-018-2944-4.
- 969 66. J. A. Villaécija-Aguilar, S. Struk, S. Goormachtig, C. Gutjahr, in *Strigolactones: Methods*  
970 *and Protocols*, C. Prandi, F. Cardinale, Eds. (Springer US, New York, NY, 2021;  
971 [https://doi.org/10.1007/978-1-0716-1429-7\\_11](https://doi.org/10.1007/978-1-0716-1429-7_11)), pp. 129–142.
- 972 67. N. Braun, A. de Saint Germain, J.-P. Pillot, S. Boutet-Mercey, M. Dalmais, I. Antoniadi,  
973 X. Li, A. Maia-Grondard, C. Le Signor, N. Bouteiller, D. Luo, A. Bendahmane, C.  
974 Turnbull, C. Rameau, The pea TCP transcription factor PsBRC1 acts downstream of  
975 Strigolactones to control shoot branching. *Plant Physiol.* **158**, 225–38 (2012).
- 976 68. M. W. Pfaffl, A new mathematical model for relative quantification in real-time RT-PCR.  
977 *Nucleic Acids Res.* **29** (2001), doi:10.1093/nar/29.9.e45.
- 978 69. T. Czechowski, R. P. Bari, M. Stitt, W. R. Scheible, M. K. Udvardi, Real-time RT-PCR  
979 profiling of over 1400 Arabidopsis transcription factors: Unprecedented sensitivity reveals  
980 novel root-and shoot-specific genes. *Plant J.* **38** (2004), doi:10.1111/j.1365-  
981 313X.2004.02051.x.
- 982 70. M. Knopkiewicz, P. Wojtaszek, Validation of reference genes for gene expression  
983 analysis using quantitative polymerase chain reaction in pea lines (Pisum sativum) with  
984 different lodging susceptibility. *Ann. Appl. Biol.* **174** (2019), doi:10.1111/aab.12475.
- 985 71. C. A. Schneider, W. S. Rasband, K. W. Eliceiri, NIH Image to ImageJ: 25 years of image  
986 analysis. *Nat. Methods.* **9**, 671–675 (2012).
- 987 72. A. de Saint Germain, G. Clavé, F. D. Boyer, in *Methods in Molecular Biology* (2021), vol.  
988 2309.
- 989 73. Z. Otwinowski, W. Minor, Processing of X-ray diffraction data collected in oscillation  
990 mode. *Methods Enzymol.* **276**, 307–326 (1997).
- 991 74. I. Lee, K. Kim, S. Lee, S. Lee, E. Hwang, K. Shin, D. Kim, J. Choi, H. Choi, J. S. Cha, H.  
992 Kim, R. A. Lee, S. Jeong, J. Kim, Y. Kim, H. G. Nam, S. K. Park, H. S. Cho, M. S. Soh,  
993 A missense allele of KARRIKIN-INSENSITIVE2 impairs ligand-binding and  
994 downstream signaling in Arabidopsis thaliana. *J. Exp. Bot.* **69**, 3609–3623 (2018).

- 995 75. P. D. Adams, P. V. Afonine, G. Bunkóczi, V. B. Chen, I. W. Davis, N. Echols, J. J.  
996 Headd, L. W. Hung, G. J. Kapral, R. W. Grosse-Kunstleve, A. J. McCoy, N. W. Moriarty,  
997 R. Oeffner, R. J. Read, D. C. Richardson, J. S. Richardson, T. C. Terwilliger, P. H. Zwart,  
998 PHENIX: A comprehensive Python-based system for macromolecular structure solution.  
999 *Acta Crystallogr. Sect. D Biol. Crystallogr.* **66**, 213–221 (2010).
- 1000 76. P. Emsley, B. Lohkamp, W. G. Scott, K. Cowtan, Features and development of Coot. *Acta*  
1001 *Crystallogr. Sect. D Biol. Crystallogr.* **66**, 486–501 (2010).
- 1002 77. W. L. DeLano, The PyMOL Molecular Graphics System, Version 2.3. *Schrödinger LLC*  
1003 (2020).
- 1004 78. J. Yang, Y. Zhang, I-TASSER server: New development for protein structure and function  
1005 predictions. *Nucleic Acids Res.* **43**, W174–W181 (2015).
- 1006 79. J. Dundas, Z. Ouyang, J. Tseng, A. Binkowski, Y. Turpaz, J. Liang, CASTp: Computed  
1007 atlas of surface topography of proteins with structural and topographical mapping of  
1008 functionally annotated residues. *Nucleic Acids Res.* **34**, W116–W118 (2006).
- 1009 80. C. Steffen, K. Thomas, U. Huniar, A. Hellweg, O. Rubner, A. Schroer, AutoDock4 and  
1010 AutoDockTools4: Automated Docking with Selective Receptor Flexibility. *J. Comput.*  
1011 *Chem.* **30**, 2785–2791 (2010).
- 1012 81. R. A. Laskowski, M. B. Swindells, LigPlot+: Multiple ligand-protein interaction diagrams  
1013 for drug discovery. *J. Chem. Inf. Model.* **51**, 2778–2786 (2011).
- 1014
- 1015
- 1016
- 1017



1018 **Figure Legends**

1019

1020 **Fig. 1. Evolutionary analysis and differential expression of the legume *Pisum sativum* KAI2s.**

1021 **(a)** Maximum likelihood phylogeny of 24 representative KAI2 amino acid sequences. Node values  
1022 represent percentage of trees in which the associated taxa clustered together. Vertical rectangles  
1023 highlight distinct KAI2 family clades. Black circle indicates legume duplication event. Pink, green,  
1024 and blue circles mark the position of PsKAI2As, PsKAI2B, and PsKAI2C respectively. The tree  
1025 is drawn to scale, with branch lengths measured in the number of substitutions per site. **(b)**  
1026 PsKAI2A, PsKAI2B and PsKAI2C are homologues to AtKAI2 and encode  $\alpha$ - $\beta$ /hydrolases.  
1027 Schematic representation of the PsKAI2A, PsKAI2B and PsKAI2C genes; Exons are in pink,  
1028 green and blue lines, non-coding sequences colored in thin black lines and UTR regions shown as  
1029 thick gray lines. Bases are numbered from the start codon. PsKAI2A shows 2 splicing variants.  
1030 Spliced introns are shown as bent (“V”) lines. Inverted triangle (▼) indicates premature  
1031 termination codons. Catalytic triad residues are indicated in pink. The hatched part indicated the  
1032 C-terminus extension of the PsKAI2.1 protein **(c-d)** Differential expression pattern of PsKAI2A  
1033 **(c, pink)** and PsKAI2B **(d, green)**. Transcript levels in the different tissues of 21 old wild-type  
1034 *Pisum sativum* plants (cv. Terese) were determined by real-time PCR, relative to PsEF1 $\alpha$ . Data  
1035 are means  $\pm$  SE (n = 2 pools of 8 plants). Inset drawing of a node showing the different parts of  
1036 the pea compound leaf.

1037

1038 **Fig. 2. Characterization of the Pskai2 mutants. (a)** Gene structure of PsKAI2 and locations of

1039 mutations. Bases are numbered from the start codon. Point mutations are indicated by dotted lines

1040 **(black and red for the one studied here) (b-d)** RT-qPCR-based expression of PsDLK2 **(b),**

1041 PsKAI2A (**c**), PsKAI2B (**d**) in roots of 10-day old *P. sativum* plants after 4 hours treatment with  
1042 solvent (Mock) or 3  $\mu$ M KAR1 or (+)-GR24 or (-)-GR24. Expression values were normalized to  
1043 those of the housekeeping gene TUBULIN (n = 3–4). Letters indicate significant differences  
1044 versus mock treatment (Kruskal-Wallis Test,  $p < 0.05$ ).

1045

1046 **Fig. 3. Arabidopsis hypocotyl elongation complementation assays with PsKAI2s.** Hypocotyl  
1047 length of 7-day-old seedlings grown under low light at 21 °C. Data are means  $\pm$  SE (n = 20-24; 2  
1048 plates of 10-12 seedlings per plate). Light blue bars: Mock (DMSO), lavender bars: (-)-GR24  
1049 (1 $\mu$ M). Complementation assays using the AtKAI2 promoter to express AtKAI2 (control) or  
1050 PsKAI2 genes in the *htl-3* mutant background (Ler ecotype) as noted above the graph. Proteins  
1051 were tagged with mCitrine or GUS protein. For DMSO controls, statistical differences were  
1052 determined using a one-way ANOVA with a Tukey multiple comparison of means post-hoc test,  
1053 statistical differences of  $P < 0.05$  are represented by different letters. Means with asterisks indicate  
1054 significant inhibition compared to mock-treated seedlings with \*\*\* corresponding to  $p \leq$   
1055 0.001 and \* to  $p \leq 0.01$ , as measured by t- test.

1056

1057 **Fig. 4. Biochemical analysis of PsKAI2A.2 and PsKAI2B interactions with different GR24**  
1058 **isomers and enzymatic property.** (a) Chemical structure of ligands used. (b) Plots of  
1059 fluorescence intensity versus SL concentrations. The change in intrinsic fluorescence of AtKAI2,  
1060 PsKAI2A.2 and PsKAI2B was monitored (see **Fig. S4**) and used to determine the apparent  $K_d$   
1061 values. The plots represent the mean of two replicates and the experiments were repeated at least  
1062 three times. The analysis was performed with GraphPad Prism 7.05 Software. (c-f) DSF assay.  
1063 The melting temperature curves of 10  $\mu$ M PsKAI2A.2 (**c, e**) or PsKAI2B (**d, f**) with (+)-GR24 (c-

1064 d), (-)-GR24 (**e-f**) at varying concentrations are shown as assessed by DSF. Each line represents  
1065 the average protein melt curve for three technical replicates; the experiment was carried out twice.  
1066 (**g-h**) Enzymatic kinetics for AtD14, AtKAI2, RMS3, PsKAI2A.2 and PsKAI2B proteins  
1067 incubated with ( $\pm$ )-GC240 (**g**) or ( $\pm$ )-GC486 (**h**). Progress curves during probes hydrolysis,  
1068 monitored ( $\lambda_{em}$  460 nm) at 25 °C. Protein catalyzed hydrolysis with 400 nM  $\mu$ M of protein and  
1069 20  $\mu$ M of probes. These traces represent one of the three replicates, and the experiments were  
1070 repeated at least twice.

1071  
1072 **Fig. 5. Comparative enzymatic activity of AtD14, AtKAI2, RMS3, PsKAI2A and PsKAI2B**  
1073 **proteins with GR24 isomers.** UPLC-UV (260 nm) analysis showing the formation of the ABC  
1074 tricycle from GR24 isomers. The enzymes (10  $\mu$ M) hydrolysis activity was monitored after  
1075 incubation with 10  $\mu$ M (+)-GR24 (yellow), (-)-GR24 (orange), (+)-2'-epi-GR24 (blue), or (-)- 2'-  
1076 epi-GR24 (purple). The indicated percentage corresponds to the hydrolysis rate calculated from  
1077 the remaining GR24 isomer, quantified in comparison with indanol as an internal standard. Data  
1078 are means  $\pm$  SE (n = 3). nd = no cleavage detected.

1079  
1080 **Fig. 6. The crystal structure of legume KAI2. (a) Overview of PsKAI2B structure.** Lid and  
1081 base domains are colored in forest and light green respectively with secondary structure elements  
1082 labeled. **(b)** Structural alignment of PsKAI2B and AtKAI2 (PDB ID: 4HTA) shown in light green  
1083 and wheat colors respectively. Root-mean-square deviation (RMSD) value of the aligned  
1084 structures is shown. The location and conservation of legume KAI2 unique residues, alanine in  
1085 position 147 (A147) and asparagine N129, are highlighted on the structure shown as sticks as well  
1086 as in reduced Multiple Sequence Alignment from **Fig. S1**.

1087

1088 **Fig. 7. Structural divergence analysis of legume KAI2A and KAI2B.** (a) Structural alignment  
1089 of PsKAI2A and PsKAI2B shown in pink and light green colors respectively. RMSD of aligned  
1090 structures is shown. (b) Analysis of PsKAI2A and PsKAI2B pocket volume, area, and morphology  
1091 is shown by solvent accessible surface presentation. Pocket size values were calculated via the  
1092 CASTp server. (c) Residues involved in defining ligand-binding pocket are shown on each  
1093 structure as sticks. Catalytic triad is shown in red. (d) Residues L/M160, S/L190, and M/L218 are  
1094 highlighted as divergent legume KAI2 residues, conserved among all legume KAI2A or KAI2B  
1095 sequences as shown in reduced Multiple Sequence Alignment from **Fig. S1**.

1096

1097 **Fig. 8. Structural basis of PsKAI2B ligand interaction.** (a) Surface (left) and cartoon (right)  
1098 representations of PsKAI2B crystal structure in complex with (-)-GR24 D-OH ring. Protein  
1099 structure is shown in blue/gray and ligand in orange. (b) Close-up view on ligand interactions and  
1100 contiguous density with the catalytic serine S95. Electron density for the ligand is shown in navy  
1101 blue and blue/gray mesh for the labeled catalytic triad. The contiguous density between S95 and  
1102 the D-OH ring indicates a covalent bond. The electron density is derived from 2mFoDFc (2fofc)  
1103 map contoured at 1.0s. (c) Side view of PsKAI2B-D-OH structure shown in cartoon with  
1104 highlighted (orange) the intact D-OH ring structure. 2-D ligand interaction plot was generated  
1105 using LigPlot+ software. Dark grey line represents S95-D-OH ring covalent bond. (d) Schematic  
1106 diagram of the proposed mechanism for the formation of the D-ring intermediate covalently bound  
1107 to S95 in a first time and then to H246.

1108

1109

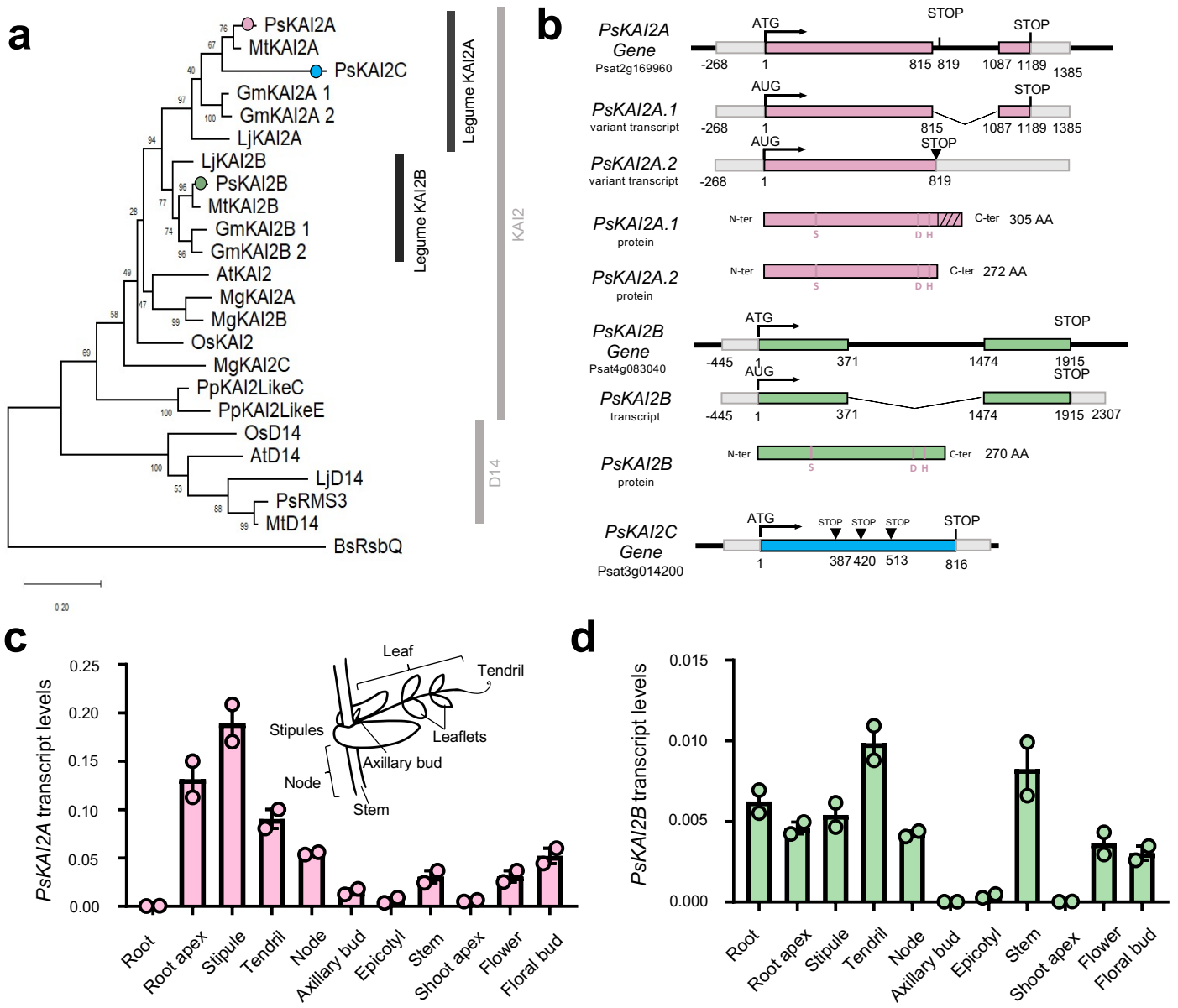


**Fig. 1**

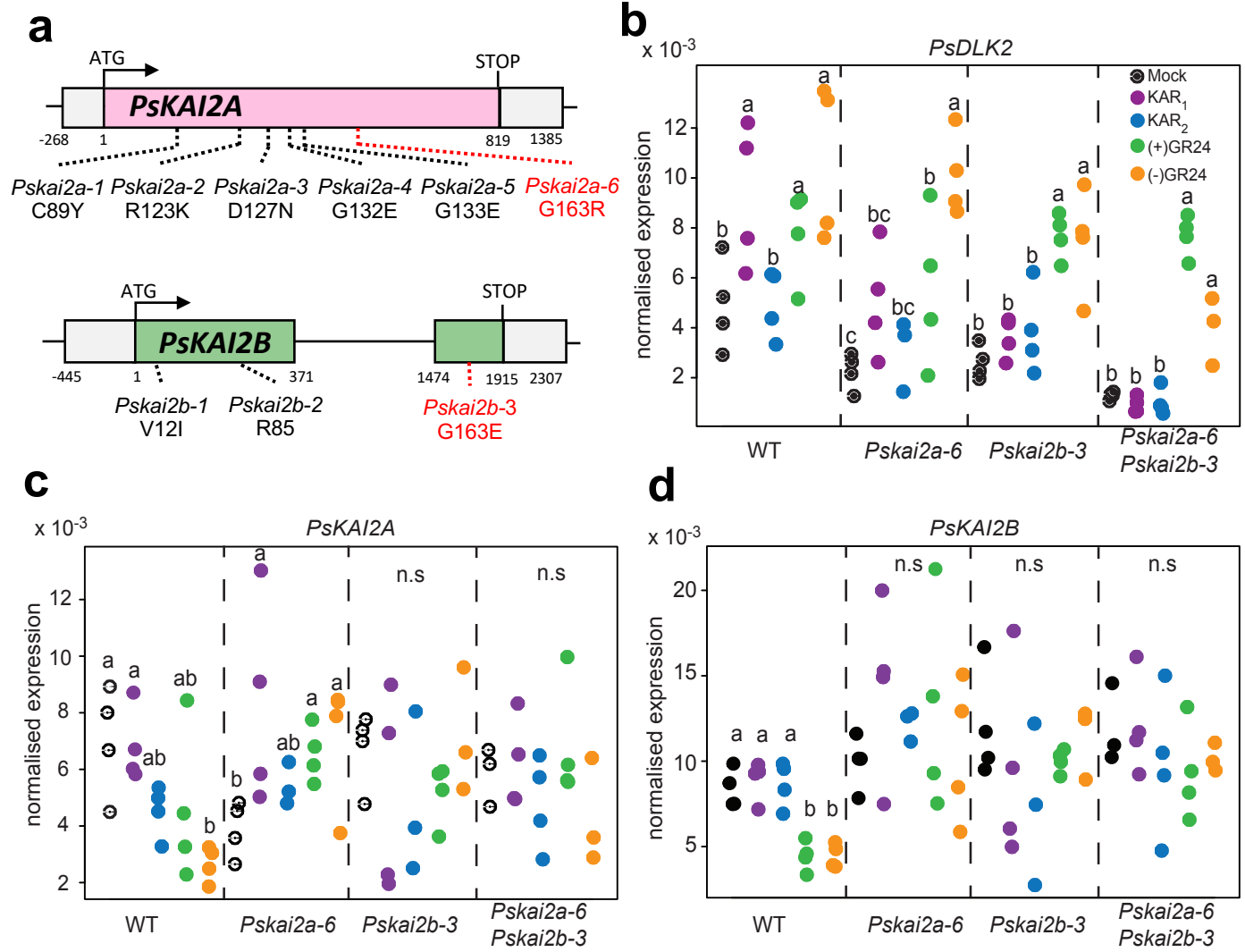


**Fig. 2**

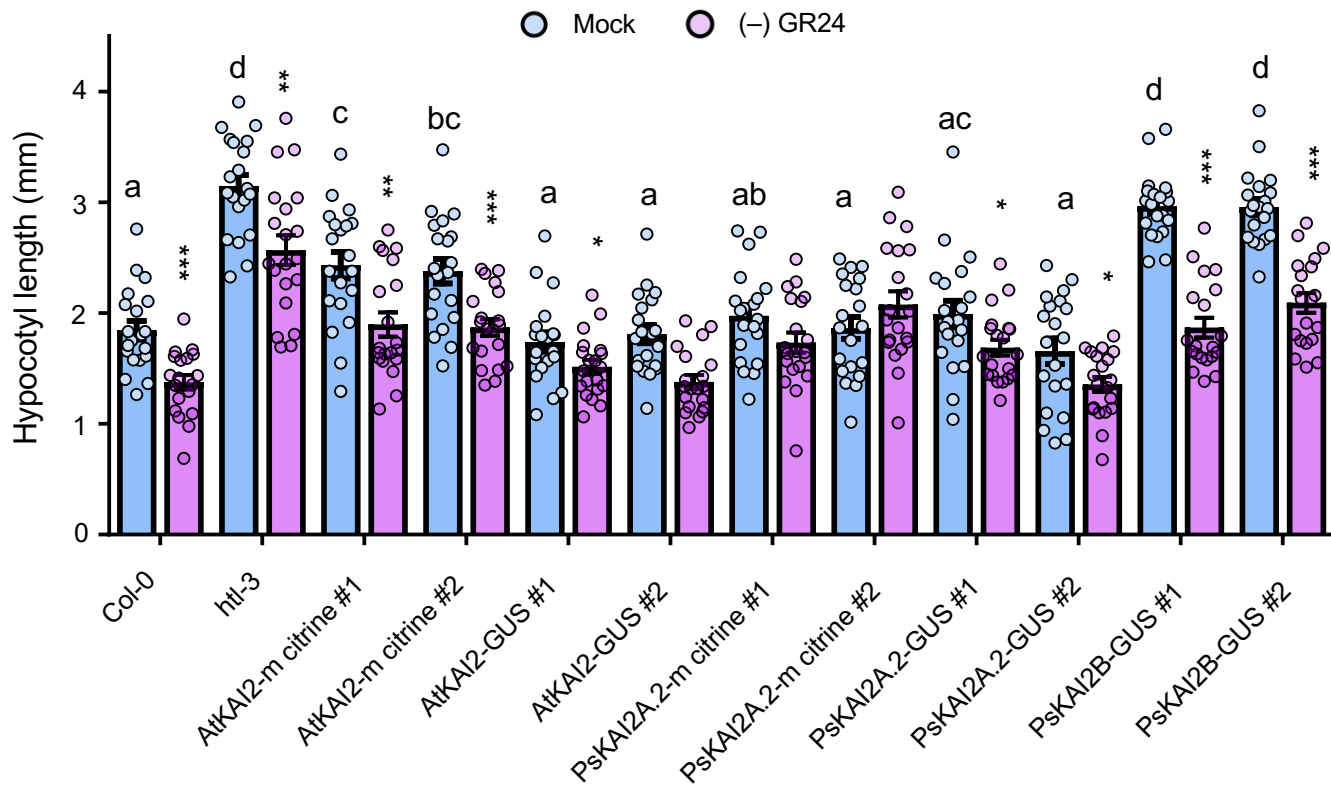


**Fig. 3**

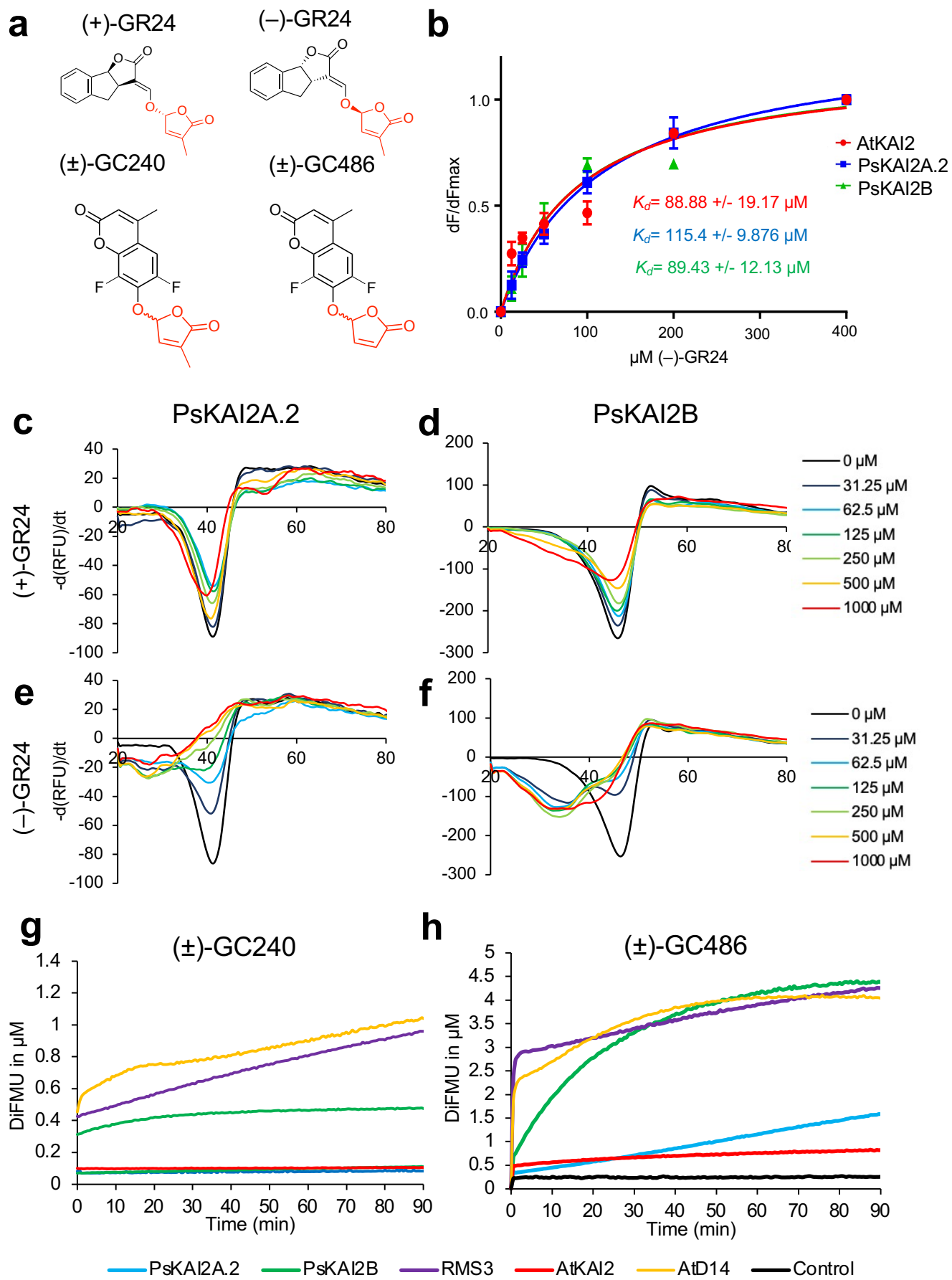


**Fig. 4**



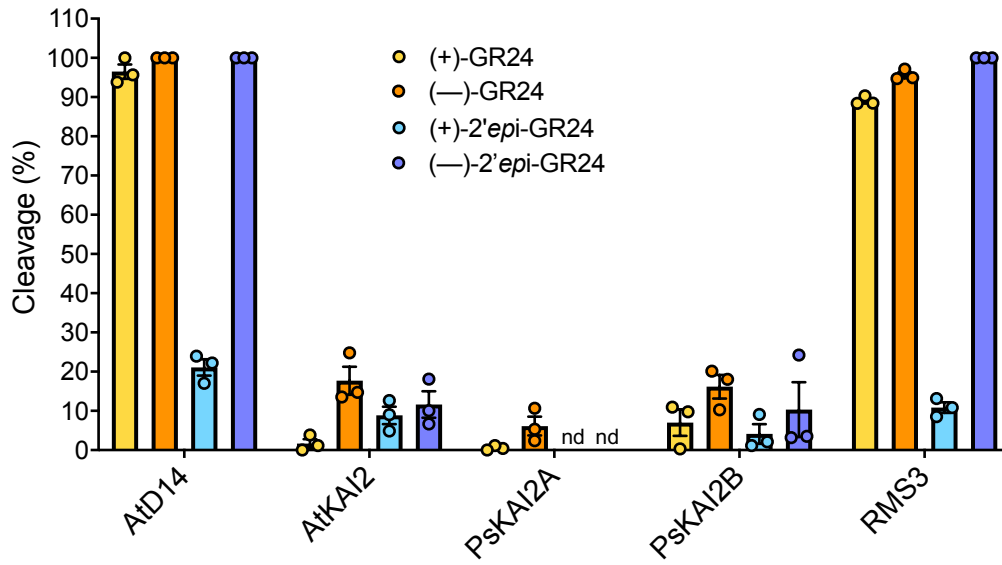


**Fig. 5**

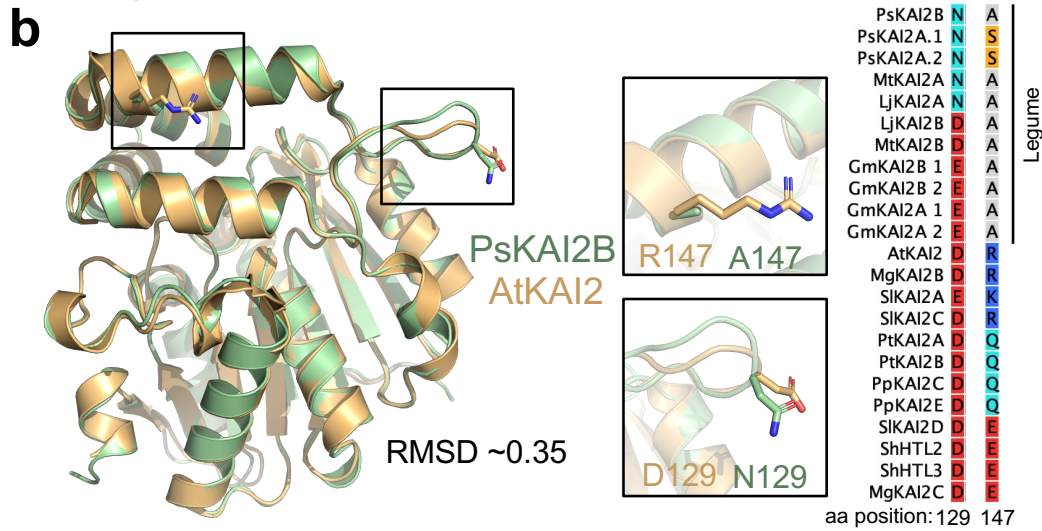
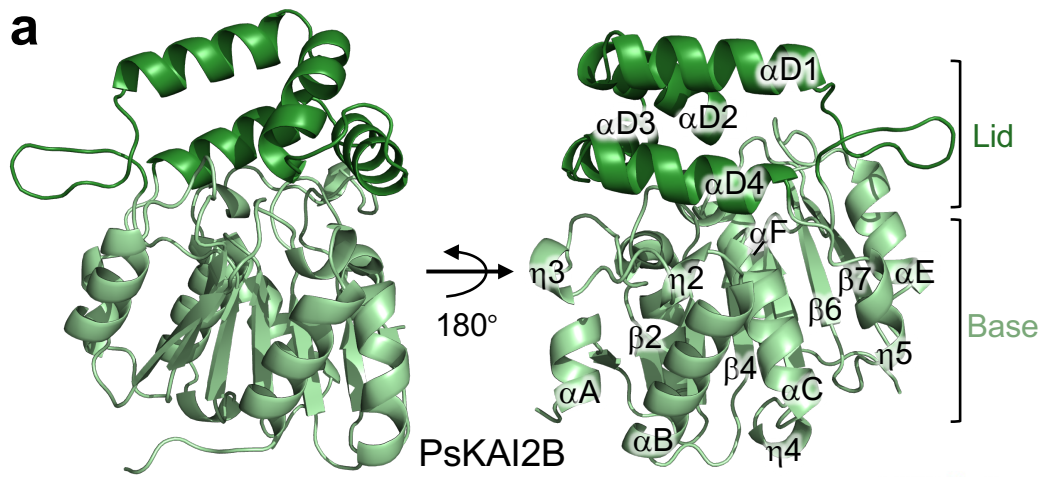


**Fig. 6**

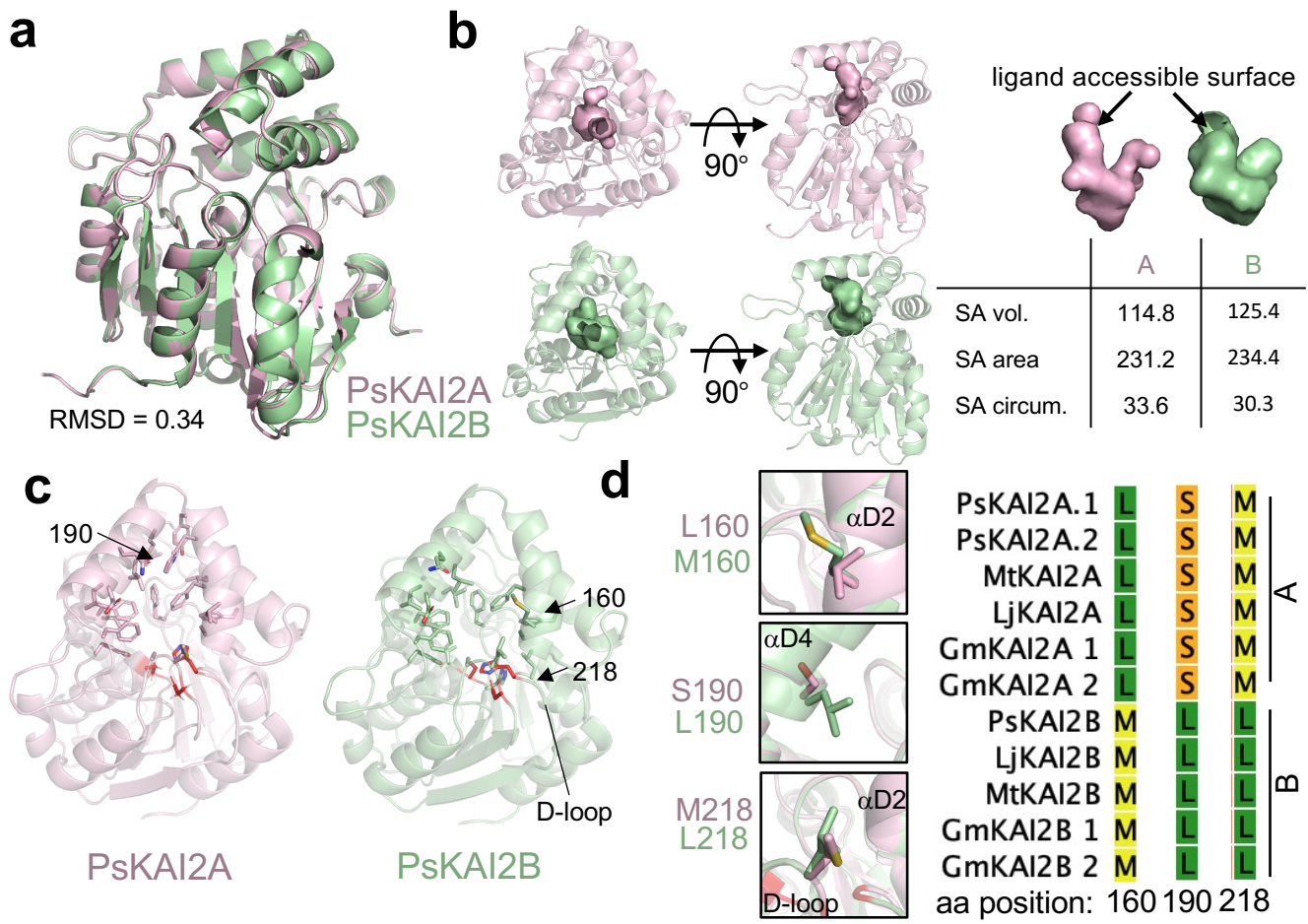


**Fig. 7**

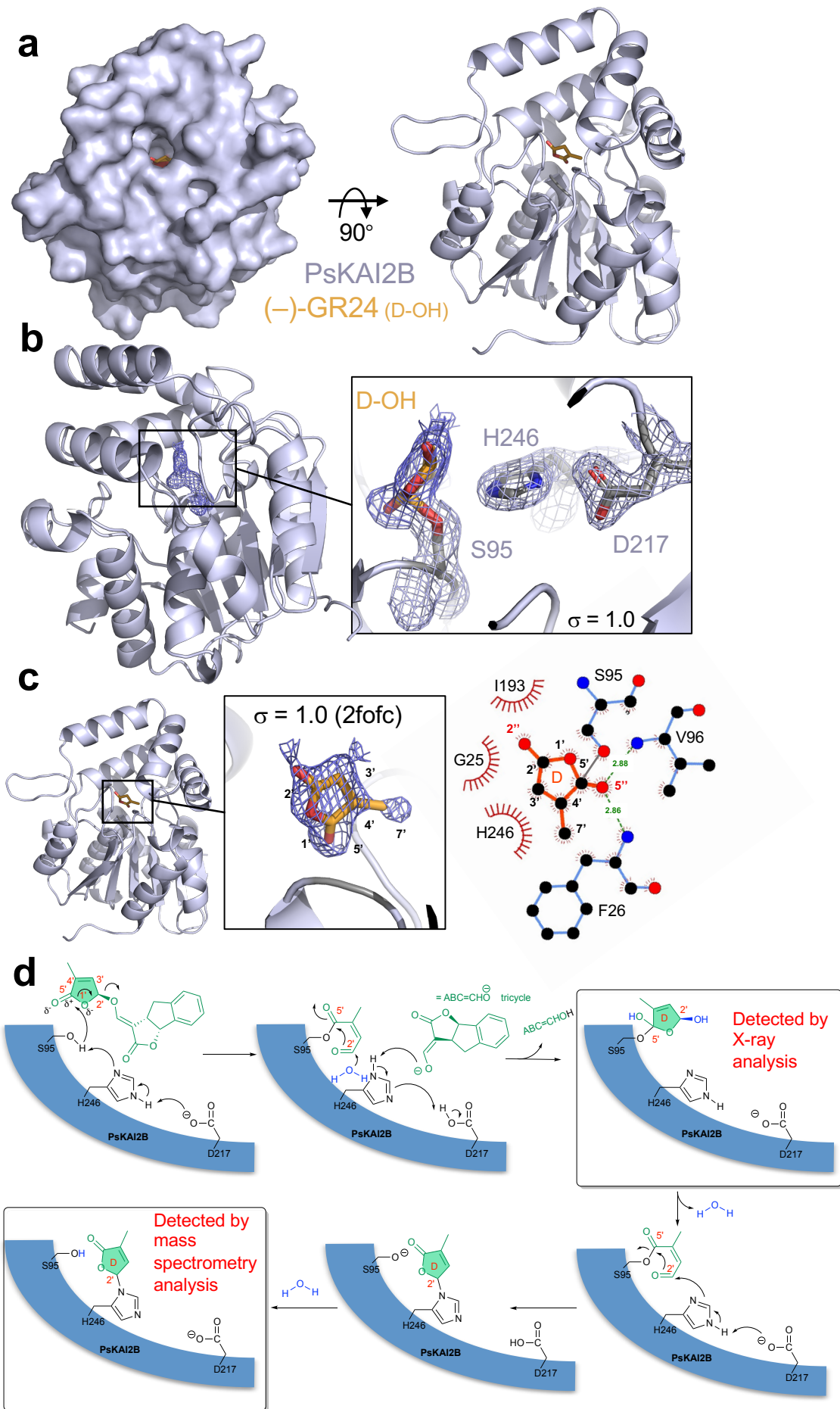


**Fig. 8**